Nanoscale

REVIEW

View Article Online
View Journal | View Issue

Cite this: *Nanoscale*, 2021, **13**, 460

Dispersant-assisted liquid-phase exfoliation of 2D materials beyond graphene

Chen-Xia Hu, Yuyoung Shin, Oliver Read and Cinzia Casiraghi *

The extensive research on liquid-phase exfoliation (LPE) performed in the last 10 years has enabled a low cost and mass scalable approach to the successful production of a range of solution-processed 2-dimensional (2D) materials suitable for many applications, from composites to energy storage and printed electronics. However, direct LPE requires the use of specific solvents, which are typically toxic and expensive. Dispersant-assisted LPE allows us to overcome this problem by enabling production of solution processed 2D materials in a wider range of solvents, including water. This approach is based on the inclusion of an additive, typically an amphiphilic molecule, designed to interact with both the nanosheet and the solvent, enabling exfoliation and stabilization at the same time. This method has been extensively used for the LPE of graphene and has been discussed in many reviews, whilst little attention has been given to dispersant-assisted LPE of 2D materials beyond graphene. Considering the increasing number of 2D materials and their potential in many applications, from nanomedicine to energy storage and catalysis, this review focuses on the dispersant-assisted LPE of transition metal dichalcogenides (TMDs), hexagonal boron nitride (h-BN) and less studied 2D materials. We first provide an introduction to the fundamentals of LPE and the type of dispersants that have been used for the production of graphene, we then discuss each class of 2D material, providing an overview on the concentration and properties of the nanosheets obtained. Finally, a perspective is given on some of the challenges that need to be addressed in this field of research.

Received 24th July 2020,
Accepted 29th November 2020

DOI: 10.1039/d0nr05514j

rsc.li/nanoscale

1 Introduction

Graphene, a single layer of graphite, is the most famous 2-dimensional (2D) material because its unique properties[1–9] make it an extremely attractive material for many applications, ranging from electronics to composites.[4,5] Since the discovery of graphene,[10] additional 2D materials have been discovered and investigated:[11–18] in nature, there are many layered materials similar to graphite, which can be exfoliated into single- and few-layers, providing 2D crystals with complementary properties to those of graphene. The family of 2D materials is continuously expanding: studies based on machine learning suggest that there could be more than 1800 2D materials available to investigate and use in various applications.[19] 2D materials have unique mechanical, electrical, optical, and magnetic properties, which are ultimately attributed to their dimensionality. Due to strong in-plane bonding and ultra-thin thickness, 2D materials exhibit excellent mechanical properties, flexibility and transparency, which are important for applications in flexible electronics.[20,21] Their high specific surface area, associated to their dimensionality, makes them useful for energy storage applications.[22,23] Furthermore, the surface chemistry of 2D materials can be easily modified by covalent or non-covalent functionalization, making them very attractive for sensing and biomedical applications.[24–27] In order to use 2D materials in real life applications, it is crucial to develop low cost and mass scalable production methods. Amongst all approaches, LPE[28–30] is one of the most attractive methods to produce solution-processed 2D materials, ideal for applications requiring large amount of 2D materials at low price and with reduced electronic grade, compared to single crystals produced by micro-mechanical exfoliation.[31] Additionally, 2D materials that cannot be directly exfoliated from a layered bulk crystal can be produced by traditional wet-chemistry techniques.[32–36] Typical applications of solution processed 2D materials include composites,[37] energy storage,[38–40] printed electronics,[41–43] and biomedical applications,[24,25,44] to give a few examples.

The LPE method was first applied to carbon nanotubes to break their bundles into individual nanotubes and to stably disperse them in a solvent,[45–50] and later applied to graphene and other 2D materials. Despite the similarities between the two materials, the different dimensionality does play an important role on the properties of the final material, *e.g.* in the case of 2D materials, the exfoliation process affects both size and thickness of the nanosheets. The extensive research into LPE

Department of Chemistry, University of Manchester, M139PL Manchester, UK.
E-mail: cinzia.casiraghi@manchester.ac.uk

of 2D materials undertaken in the last 10 years has allowed the community to achieve a detailed understanding of the fundamental processes involved in exfoliation and interaction of the 2D material with a solvent, by enabling production of a wide range of 2D material dispersions.[51] In parallel, post-processing and characterization methods have been developed and refined, allowing a fine control over the nanosheets properties.[52–57] The LPE method relies on the favourable interaction between solvent molecules and the layered crystal for stabilisation of the dispersed materials, while an external force, *e.g.* made by ultrasonication or shear mixing, is applied to exfoliate the layers. Hence, only specific solvents, for example *N*-methyl-2-pyrrolidone (NMP), dimethyl sulfoxide (DMSO), and *N*,*N*-dimethyl formamide (DMF), have been shown to be effective at exfoliating layered materials.[30,58] Typically, these solvents are toxic and expensive. Water, on the other hand, is not effective at exfoliating graphite. Increasing the temperature during sonication has been reported to help exfoliation,[59] but the concentration reported is still very low. Nevertheless, biomedical applications and many others do require this solvent. Furthermore, in the next few years, a strong reduction in the use of toxic solvents in industrial processes is expected due to policy changes related to sustainability issues. The use of dispersants ("exfoliating agents" or "stabilizers") in LPE allows to extend the number of solvents available, including water, for the production of stable and concentrated dispersions. In addition, this method allows the surface charge and chemistry of the nanosheets to be tuned, simply by selecting the dispersant. While extensive reviews on dispersant-assisted LPE of graphene have been already reported in literature,[56,60,61] little attention has been dedicated so far to dispersant-assisted LPE of 2D materials beyond graphene. Considering the increasing interest in 2D materials and the advantages of dispersant-assisted LPE, here we aim at providing an overview on the different strategies used in the dispersant-assisted LPE of 2D materials beyond graphene. Since the chemical structure of other 2D materials is different from that of graphene, a dispersant that is very effective at producing graphene, may not be a good dispersant for other 2D crystals, hence it is important to consider each 2D material separately. We will focus on the most intensively investigated 2D materials, such as the family of 2D TMDs, h-BN and black phosphorous (BP). We have found more than 50 works published, mostly on TMDs. A small number of works have been also found on less studied 2D materials, such as antimonene, and reported in the last part of this review. Fig. 1 shows an overview of the class of materials covered in this review. For each material, we will describe the results obtained based on the type of dispersant used, as introduced in section 2, and we will provide a detailed description on the properties of the obtained dispersions. We conclude this review with a perspective on some of the challenges that need to be addressed in this research area and by highlighting the advantages and disadvantages of the dispersant-assisted LPE method.

2 Dispersant-assisted LPE

2.1 Fundamentals of the LPE

The most used exfoliation technique is based on ultra-sonication, where the layered materials are exfoliated by the microjets and shock waves generated by the collapse of the liquid cavitation-induced microbubbles.[62] Alternatively, a shear mixer such as a high-shear mixer or even just a kitchen blender, can be used: in this case, the exfoliation mechanism is mainly dependent on high shear force with aid of collision and

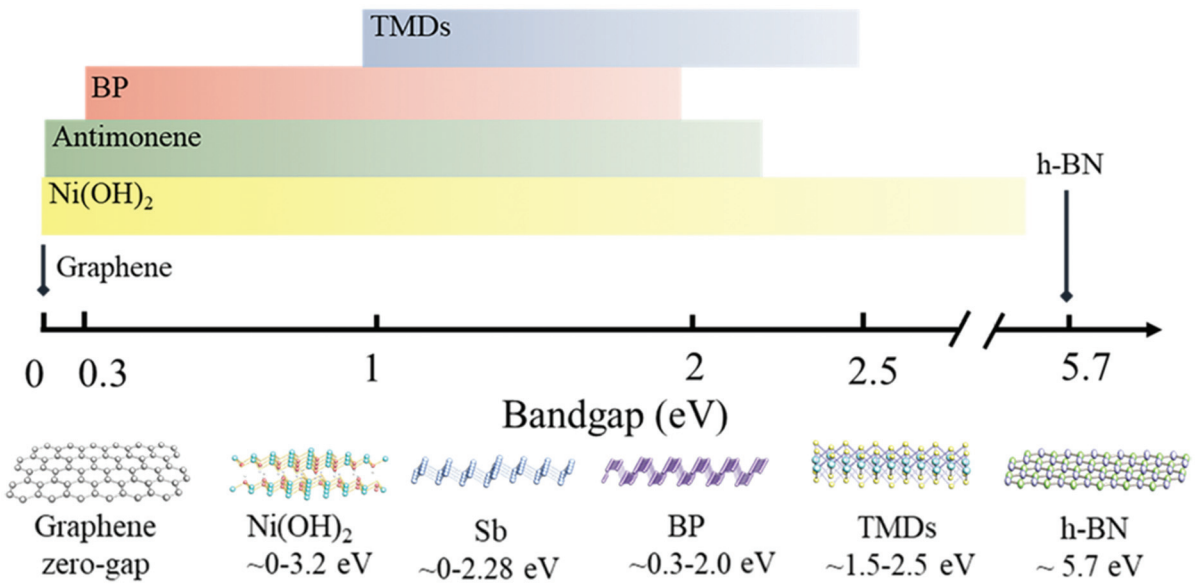

Fig. 1 Schematic showing the atomic structure and band gap of some of the 2D materials selected for this review. The 2D material family is composed by hundreds of crystals with different properties, ranging from metallic to semiconducting and insulating crystals.

cavitation.[62,63] Here we will focus on works based on these exfoliation methods, although there are also other types of LPE approaches based on high shear force, such as ball-milling[64,65] and microfluidization.[66] Different exfoliation techniques, including those already mentioned and also variation of those methods, have been extensively investigated, but a detailed discussion of all the processes is beyond the scope of this review and can be found in other reviews.[51,56,60,67]

The general LPE experimental procedure can be described as follows: the bulk layered material, typically in powder form, is first added to either a pure solvent or dispersant-containing solution, followed by an exfoliation step performed by applying ultrasonic and/or shear energy; then exfoliated thin nanosheets and un- or incompletely-exfoliated thick layered materials, contained in the obtained dispersion, are separated, typically by using centrifugation or natural sedimentation over time by gravitational force. Finally, the supernatant, containing well-dispersed and thin nanosheets, is collected. Fig. 2 shows the schematic of the process. For both exfoliation and stabilization, it is of critical importance to select an appropriate liquid medium since the exfoliation and stabilization of the 2D crystal nanosheets is dependent on the interfacial interaction between the exfoliated 2D crystal nanosheets and the liquid medium.[58,68,69] The simplest way of describing the stabilization mechanism would be based on the "like dissolves like" rule in chemistry, *i.e.* when the surface energy of the solute matches that of the solvent, the enthalpy of mixing, ΔH_{mix}, is small, hence the mixing of solute in a solvent is determined by the changes in entropy (ΔS_{mix}). The free energy of mixing, ΔG_{mix}, is defined as:[70]

$$\Delta G_{mix} = \Delta H_{mix} - T\Delta S_{mix} \quad (1)$$

For typical molecular solutes, the entropy of mixing can be large enough to drive spontaneous mixing process and the mixture is considered as a solution. In the case of 2D crystals with sizes in the range between several tens of nanometers to microns, ΔS_{mix} is not large enough to spontaneously drive the process.[45] Therefore, ΔH_{mix} needs to be minimized by careful selection of the solvent to enable the exfoliated 2D crystals to be stably dispersed in the solvent and to prevent re-stacking.[45] The best solvents for LPE are typically organics as they have shown to produce graphene dispersions with high yield and stability.[30,58] Those solvents have a surface tension of ~40 mJ m^{-2}, hence they show favourable interactions with graphene, which has a similar surface tension value.[30,58] It should be noted that the surface energies of liquids are ~30 mJ m^{-2}, which is *ca.* 0.1 mJ m^{-2} K^{-1} higher than their surface tension estimated using a universal value for surface entropy.[46,71] Some of the most studied 2D materials, such as h-BN, MoS_2 and WS_2, also show good exfoliation efficiency in these solvent types (Fig. 3).[29,56,67] It should be noted that throughout this review, the term 'exfoliation efficiency' is used to refer to the amount of the dispersed nanosheets in the solution, determined by the final concentration, measured by UV-Vis spectroscopy. This term does not refer to the efficiency of delamination, which is usually obtained by the characterization of the thickness of nanosheets by atomic force microscopy (AFM).

The simple model based on surface tension as a measure of dispersability of 2D materials is useful to find the optimal solvent medium in general, but it does not elucidate the detailed interaction between the solvent molecules and the nanosheets. A model that does take into account of those interactions is based on the use of the Hildebrand and Hansen solubility parameters, in which the intermolecular interactions are divided into three types: dispersive (D), polar (P) and hydrogen-bonding (H) components.[29,45,58,68] The Hildebrand solubility parameter, δ_T, is the square root of the cohesive energy density, $E_{C,T}/V$, where $E_{C,T}$ is the total molar cohesive energy and V is the molar volume of the solvent. The Hansen solubility parameters, δ_i (i = D, P, and H), are the square root of the cohesive energy density of each component. The square of Hildebrand solubility is therefore, the sum of the squares of each Hansen solubility parameters:[29,45,58,68]

$$\delta_T^2 = \delta_D^2 + \delta_P^2 + \delta_H^2 \quad (2)$$

The dispersability of a 2D material in a solvent is optimal when both the solvent and the 2D material share similar values for all three Hansen solubility parameters. By exfoliating graphene in 40 solvents, it was shown that solvents with well-defined values of the Hansen solubility parameters produce better exfoliation and stabilization.[68] The work was then extended to 2D materials beyond graphene: h-BN, MoS_2 and WS_2 all show a very sharp peak in the Hansen parameters plot *vs.* concentration. In Fig. 3, the dispersive Hansen parameter *vs.* concentration plots for those 2D materials are shown as representative Hansen solubility parameter plots since the dispersive interaction is typically the strongest interaction

Fig. 2 Schematic of the production of 2D nanosheets by liquid-phase exfoliation. The process consists of providing energy *via* sonication or shear mixing, followed by centrifugation and collection of the material.

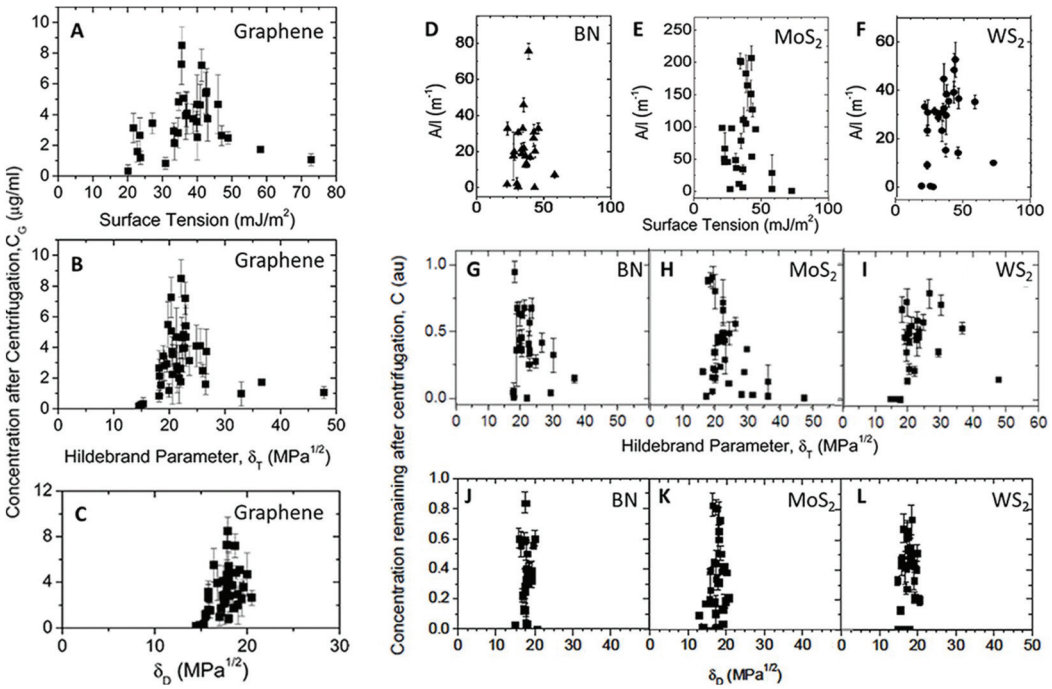

Fig. 3 Dispersion concentrations for a range of solvents plotted for graphene *versus* (A) solvent surface tension (B) Hildebrand parameter, δ_T, and (C) dispersive Hanson solubility parameter, δ_D. The graphene dispersion concentrations were determined using absorbance at 660 nm using absorption coefficient of 2460 L g^{-1} m^{-1}. Dispersion concentrations for a range of solvents plotted *versus* (D–F) solvent surface tension (G–I) δ_T and (J–L) δ_D for BN, MoS_2 and WS_2, respectively. (D–L) The 2D crystal dispersion concentrations were plotted as absorbance divided by cell length, *A*/*l*. Reproduced from ref. 29 and 68 with permission from American Association for the Advancement of Science and the American Chemical Society.

component. For other Hansen solubility parameter *vs.* concentration plots we invite the reader to refer to ref. 29 and 68. This demonstrates that successful exfoliation and stabilisation of dispersions require optimization of all the interaction energies.[29] The Hansen parameters are particularly useful not only for finding new solvents (the parameters are known for more than 1200 solvents[72]) but also to identify the best mixed solvent solutions.[73] Coleman *et al.*[29] suggested that the best 3 solvents for LPE of h-BN are: cyclohexyl-pyrrolidinone, *N*-dodecyl-pyrrolidone and benzyl benzoate, while NMP is not very efficient. Note that in contrast to graphite, h-BN can be exfoliated in water,[74] but the concentration is not very high. Hence h-BN dispersions are usually made in a mixed solvent or in water with a dispersant. In the case of MoS_2 and WS_2, solvents such as NMP, DMSO and DMF work very well.[29]

Stabilization is typically achieved electrostatically, hence this process can be described by the Derjaguin–Landau–Verwey–Overbeek (DLVO), which predicts stability effects that are electrical in origin in charged colloidal particles.[75] Briefly, in the DLVO theory, stabilization is achieved by the balance between repulsive electrostatic interaction from charges surrounding the particles and van der Waals attractive interaction. The total interaction energy is characterized by two minima: a primary minimum (at very short distances) associated to aggregation, and a secondary minimum, at relatively large inter-particle distances, associated to flocculation. In between the minima, *i.e.* at a certain distance, a potential barrier is generated that prevent nanoparticles from aggregation. The higher barrier the system obtains the better the stability. The barrier height can be tuned by external parameters, such as the concentration and type of electrolyte and the pH.

2.2 Types of dispersants for assisted LPE

Although organic solvents are very effective at LPE of 2D materials, they have several disadvantages, including high cost, high boiling point and toxicity. Water is the most suitable choice of solvent for many applications as it is abundant, low cost and environmental friendly. However, since many layered materials are insoluble or have low solubility in water, an additive is typically needed to perform LPE in this solvent. This method is named: "dispersant-assisted LPE". Note that dispersants can also be used in combination with other solvents, not only with water: if the dispersant is carefully selected, a higher exfoliation yield can be achieved, in comparison to the yield obtained using only the solvent.[28,76–82] In this review, we will focus mostly on dispersant-assisted LPE in water. In this framework, all dispersants used are amphiphilic, *i.e.* they are composed by a hydrophobic part that allows the molecule to adsorb onto the surface of the nanomaterial and a hydrophilic component, which allows interaction with water, allowing stabilization of the material. However, the exfoliation

efficiency, *i.e.* the amount of material exfoliated, can dramatically change depending on the specific interactions of the dispersant with the solvent and with the nanosheets, hence not all amphiphilic molecules are effective at LPE. Here we consider only the most used dispersants, divided into three groups: surfactants, macromolecules, and small aromatic molecules. Table 1 shows examples of some of the most used dispersants.

(i) Surfactants: surface active agents, or so-called surfactants, are amphiphilic molecules that are typically adsorbed at the solvent interface (*e.g.* water/air or water/oil), reducing the surface tension.[83] Their structure consists of a hydrophobic tail, typically in the form of a carbon chain, and a hydrophilic head, from which the surfactant is classified as non-ionic, ionic and zwitterionic. Due to their amphiphilic nature, the surfactant molecules adsorb at the interface orienting the hydrophobic chains in the hydrophobic medium and the hydrophilic head group in the hydrophilic medium, thus reducing the intermolecular forces at the interface, *i.e.* reducing the surface tension. With increasing solute concentration, the surface tension decreases until the surfactant molecules form a monolayer at the interface, at which point, known as "the critical micelle concentration" (CMC), the excess molecules self-assemble into small aggregates, called "micelles". The high solubility of the micelles is commonly used to solubilize insoluble materials by incorporating them into the micelle. Hence, surfactants are crucial components in detergents and are widely used by many industries. The same approach was successfully extended to disperse insoluble nanomaterials in water, *e.g.* dispersions of individual carbon nanotubes in water were successfully demonstrated in 2002.[84] The method was then successfully extended to graphene.[85] In these cases, surfactants adsorb *via* hydrophobic and van der Waals interactions, while the hydrophilic groups extend into the aqueous solvent. Depending on their type, ionic/polar or non-ionic, re-aggregation of the dispersed nanomaterials can be prevented through electrostatic or steric repulsion, respectively. The first work on surfactant-assisted LPE of graphene was produced by using sodium dodecyl benzene sulfonate (SDBS) and sodium cholate (SC).[85–87] However, a relatively low exfoliation efficiency was observed, even after extensive sonication. Furthermore, the CMC value was observed to be an optimal surfactant concentration for LPE.[87,88] However, a recent work[89] has shown that no clear correlation between CMC value or surfactant type and exfoliation efficiency exists, as discussed in section 3.

(ii) Macromolecules: this class of material include polymers, which consist of repeating subunits (monomers). Note that some polymers are also classified as surfactants, but in this review, we distinguish between the two cases, as polymers are characterized by much higher molecular weight, higher repulsive barrier due to the long tails as well as stronger surface adsorption, compared to traditional (*i.e.* monomeric) surfactants, discussed in the previous section. The typical stabilization mechanism is steric: the adsorbed polymer chains extend into the solvent. When two nanosheets get too close to each other, the polymer chains share the same space, leading to reduced number of conformations and increase in free energy of the system, contributing to the nanosheets repulsion. Other effects such as osmotic pressure and lyophilic interactions further contribute to prevent re-aggregation. In the case of ionic polymers, electrostatic stabilization will also play a role. May *et al.*[90] provided an expression for the free energy of adsorption of polymer chains onto the surface of nanosheets in a solvent environment as a function of the Hildebrand solubility parameters of the solvent, polymer, and nanosheets. The model, in agreement with the experimental data, shows that the most concentrated and stable dispersions are obtained when the polymer and solvent solubility para-

Table 1 Examples of the most used dispersants for liquid phase exfoliation of graphene. The dispersants type ranges from small-molecule surfactants, macromolecules and small aromatic molecules

Dispersant	Chemical structural formula
Small-molecule surfacant	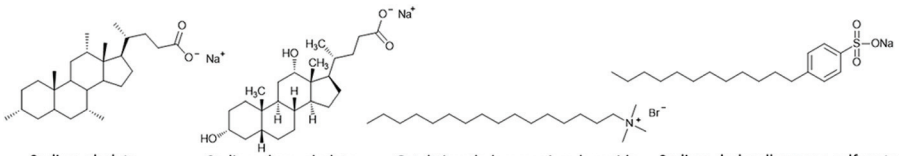 Sodium cholate (SC); Sodium deoxycholate (SDC); Cetyltrimethylammonium bromide (CTAB); Sodium dodecylbenzene sulfonate (SDS)
Macromolecule	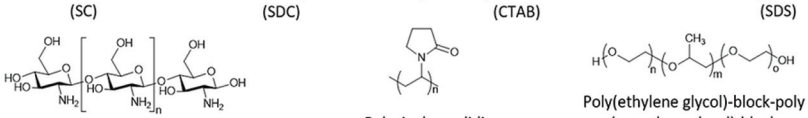 Chitosan; Polyvinylpyrrolidine (PVP); Poly(ethylene glycol)-block-poly-(propylene glycol)-block-poly(ethylene glycol) (Pluronic® P-123)
Small aromatic molecule	 1-Pyrenesulfonic acid sodium salt (PS1); 1-Pyrenebutyric acid (PyBA); 1-Aminopyrene (Py-NH_2)

meters match. In addition, the model describes both the peak width and the dependence of nanosheet concentration on polymer molecular weight.[90] Note however, that this model focuses on London interactions only, so it cannot be extended in polar or hydrogen bonding solvent system.[90] A large range of polymers has been used as exfoliation agent for LPE. Selected works include the use of hydrophilic polymers containing polyvinylpyrrolidone (PVP) and poly(ethylene oxide) (PEO), which have been used to increase graphene concentration from 0.5–1.0 mg mL^{-1} (without dispersant) to 2.6 mg mL^{-1} (with dispersant).[91–93] Biopolymers, *i.e.* natural polymers produced by living organisms, such as plants or microbes, are extremely attractive, compared to artificial ones, because of their reduced cost, abundance, possible biodegradability and improved sustainability. This class includes a very large number of materials such as collagen, silk fibroin, gelatine, starch, cellulose, alginate, polyester, polycarbonates, polyamides, vinyl polymers, proteins, nucleic acids, polysaccharides, and deoxyribonucleic acid (DNA), to give a few examples. Amongst biopolymers, polysaccharides such as chitosan (CS) and alginate have been exploited for LPE, producing water dispersible graphene by LPE.[94,95] Lignin and tannic acid natural polymers were also reported to produce aqueous graphene dispersion.[96,97] In the case of biomolecules, proteins like bovine serum albumin (BSA), peptides, nucleotides, ribonucleic acid and DNA have been widely reported in literature for exfoliation of graphite in water. For an extensive review on the use of these type of dispersants, we invite the reader to look at ref. 98.

(iii) Small aromatic molecules: polyaromatic hydrocarbons (PAH) have been shown to be promising exfoliating agents for high-yield exfoliation of graphite, through effective adsorption of the PAH base onto the graphene surface through π–π interaction.[43,60,99–101] The exfoliation mechanism by PAHs has been initially explained by the "molecular wedging effect", *i.e.* by the ability of pyrene to "intercalate" between the layers during exfoliation.[102] Although this could be a reasonable explanation, no experimental or theoretical study has fully confirmed this mechanism. Various types of PAH derivatives were investigated including anthracene,[103] coronene,[104,105] perylene[106] and diazoperipropyrenium,[107] showing their ability to effectively exfoliate graphene in water through either electrostatic repulsion or steric hindrance from the functional groups. The most studied PAH derivatives belong to the class of pyrene derivatives.[43,60,99,100,108–113] The effect of different functional groups of pyrene on the graphene exfoliation yield has been widely investigated.[99,108,110,114] In particular, Parviz *et al.*[99] made a detailed comparative study between surfactants, polymers and pyrene derivatives as dispersants for assisted LPE, demonstrating that the graphene/stabilizer yield obtained by pyrene derivatives is exceptionally high relative to conventional nanomaterial stabilizers, such as SDBS and PVP, under the same experimental conditions (Fig. 4A). Hence, a given graphene dispersion quality can be achieved at far lower mass

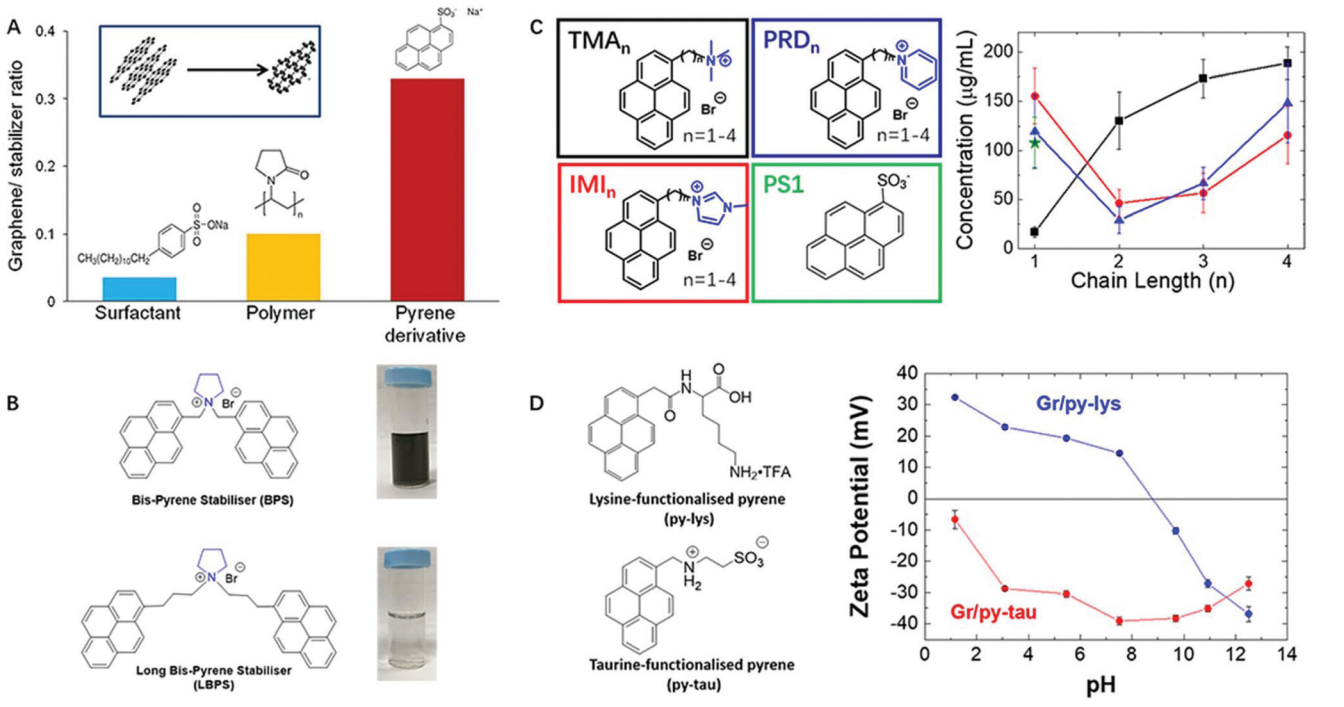

Fig. 4 Exfoliation of graphene with pyrene derivatives. (A) Graphene/stabilizer ratio when using different dispersants including SDBS, PVP and PS1. (B) Pyrene derivatives molecular structures and the digital images of graphene dispersions fabricated with their assist. (C) Left panel: Molecular structure of four pyrene derivatives. Right panel: Graphene dispersions concentration *vs.* pyrene derivatives with increasing carbon chain length. (D) Pyrene derivatives molecular structures and corresponding assisted graphene dispersions zeta potentials measured under different pH value. Reproduced from ref. 99, 109, 110 and 115 with permission from the American Chemical Society and Royal Society of Chemistry.

content of pyrene derivatives than polymers or common surfactants, enabling the production of dispersions of high quality for applications in nanocomposites, films, and electronic devices, due to the lower amount of undesirable stabilizer molecules.[99] Indeed, this methodology has been successfully used to produce highly concentrated and stable 2D material based inks for printable electronics.[43] In the same study,[99] it was observed that the exfoliation yield strongly depends on the type of pyrene derivative used. As the exfoliation mechanism is not fully understood, it is very important to clarify how to design the pyrene derivative providing the highest exfoliation efficiency. Parviz *et al.* suggested that the use of more electronegative functional groups, *e.g.* sulfonyl group, should provide better exfoliation efficiency by decreasing the electron density on the pyrene basal plane and thus increasing the affinity of the pyrene base with graphene surface by accepting electrons.[99] However, Schlierf *et al.*[108] reported a systematic study based on the use of pyrene derivatives with increasing number of sulfonic groups, which showed that pyrene functionalized with four sulfonic groups is not efficient at exfoliating graphene, due to its high solubility in water. It is clear from these studies that the exfoliation efficiency of the pyrene derivative is determined by the balance of the interactions between graphene, water and the dispersant. If the interactions of the dispersant with the water molecules are stronger than the interactions of the dispersant with graphene, then adsorption of the dispersant into graphene will be poor, giving a low exfoliation efficiency. This study[108] clearly demonstrated that higher solubility is not correlated to higher exfoliation yield and that the exfoliation mechanism is much more complex. A follow up study[115] performed in our group demonstrated that high solubility is a not a mandatory requirement for a pyrene derivative to be an efficient dispersant. In our work a bis-pyrene stabiliser (BPS), functionalized with a pyrrolidine central group, Fig. 4B, was used as dispersant and its exfoliation efficiency was compared to that of the most used pyrene derivative, 1-pyrenesulfonic acid sodium salt (PS1). Although BPS is insoluble in aqueous media (the solubility of BPS is under the detection limit of nuclear magnetic resonance), this dispersant showed exfoliation efficiency up to 3–5 times higher than that obtained with PS1. The enhanced exfoliation efficiency of BPS has been attributed to the higher interaction strength between BPS and graphene, compared to the interaction of BPS and graphene with water. This interaction strength is related to the strong π–π interactions from the two pyrene binding groups, which also makes BPS insoluble in water, further enhancing its adsorption onto graphene. This work showed that self-assembling of two insoluble nanomaterials can be used as approach to solubilize the resulting hybrid material, by carefully tuning the interactions between water, graphene and dispersant. In another recent work from our group,[110] a detailed experimental and theoretical analysis on the use of pyrene derivatives with different functional groups was presented. In the case of pyrene derivatives with an aromatic functional group, we observed that this type of functional group is not only involved in solubilization in water, but also in adsorption on the graphene surface, showing much more complicated mechanism in exfoliation/stabilization of graphene nanosheets than the functional groups with localized charge, which shows simple solubilization mechanism. Another design element that strongly determines the exfoliation efficiency of the pyrene derivative is the distance of the functional group from the pyrene core. Parviz *et al.* compared two pyrene derivatives functionalized with a carboxyl group, where one had a butyl chain linker, whereas the other was directly bonded.[99] Their results suggested that at high concentration of the dispersants, a longer distance between the basal plane and the surface charge would provide better π–π interactions, by reducing the density of electrons on the pyrene plane.[99] However, in this case, the comparison of exfoliation efficiency was drawn from a very small difference in the final graphene concentration, almost within the range of the experimental error. Heard *et al.*[111] also presented a similar comparative study, but with sulfonic functional groups instead. Their study showed that the exfoliation efficiency almost doubled when using a longer linker group, concluding that longer distances between the functional group and the pyrene provide more efficient adsorption of the pyrene on graphene as well as better solvation of the polar group, resulting in enhanced exfoliation. A more systematic study was performed by our group,[110] who introduced an incremental increase of the alkyl spacer, showing that the effect on the exfoliation efficiency is determined by a balance between the chain length and the functional group, Fig. 4C. In general, a longer chain reduces steric hindrance of the functional group on the pyrene adsorption and increases thermodynamic stability of the solvation of polar groups, when the charge is localized. Finally, amphoteric pyrene derivatives have also been used for production of charge-tuneable graphene dispersions, whose surface charge is controlled by the pH (Fig. 4D).[109] One of the main advantages of using pyrene derivatives as dispersants is, in addition to the high exfoliation efficiency, their ability to produce biocompatible 2D materials.[43] Although pyrene is toxic in relatively high concentrations, pyrene derivatives did not show any cytotoxicity effect, once adsorbed onto the nanosheet,[43,110] although the exact biocompatibility (*i.e.* the maximum dose) depends on the type of pyrene used: graphene obtained by BPS, for example, has shown some cytotoxic effects, depending on the initial concentration used, in contrast to graphene produced by PS1. In general, graphene produced by cationic pyrene derivatives shows excellent colloidal stability in the cell culture medium and exceptional biocompatibility and high internalization in both non-cancer and cancer cell lines, making cationic graphene very attractive for biomedical applications.[110]

3 State of art

3.1 Transition metal dichalcogenides

TMDs is a general name for the class of layered materials with chemical formula MX_2, where M refers to the transition metal

element and X refers to the chalcogen element. The monolayer TMD contains three atomic layers, where the upper and lower chalcogen layers and the intermediate transition metal layer form a sandwich structure. Similar to graphene, the TMD monolayers are stacked by van der Waals forces to form layered bulk TMDs.[116] In TMDs, the different coordination modes between M and X will cause different crystal polytypes, such as 2H-, 1T-, 1T′-, and 3R-type. Different crystal polytypes show different stability. For example, in the 2H-type MoS_2 atoms stack with a S–Mo–S' sequence in hexagonal closed packing mode, which is thermodynamically stable and therefore found as bulk crystal in nature. TMDs were first exfoliated into nanosheets *via* LPE in NMP, reaching concentrations of 0.3 mg mL^{-1} and 0.15 mg mL^{-1} for MoS_2 and WS_2, respectively.[29] In the same year, exfoliation of six different TMDs, including MoS_2, WS_2, $MoTe_2$, $MoSe_2$, $NbSe_2$ and $TaSe_2$ using SC in water was reported.[116,117] In this work, bulk materials were exfoliated in aqueous surfactant solution by probe sonication for 30 min, reaching a concentration of up to 0.048 mg mL^{-1}. It was also shown that the concentration can be increased to 0.5 mg mL^{-1} by increasing sonication time up to 16 hours. The exfoliated MoS_2 nanosheets show thickness between 2 to 9 layers and average lateral size of around 280 nm. A follow-up study on the use of SC was reported:[118] the authors noticed that the B-exciton intensity and A-exciton position of MoS_2 nanosheets were sensitive to surfactant concentration, when other parameters were fixed. As the position and the oscillator strength of the excitons' peaks have been observed to change with the lateral size and thickness of the nanosheets, respectively,[119] this result indicates that the surfactant concentration directly affects the properties of the nanosheets. In this study,[118] a fixed concentration of bulk MoS_2 was added in aqueous solution made with different concentrations of SC and exfoliated with a shear mixer. It was observed that all processing parameters (the MoS_2 concentration, the mixing time, the liquid volume, and the rotor speed) influence the concentration and also the production rate. Concentrations as high as 0.5 mg mL^{-1} and production rates of ~1 mg min^{-1} were achieved. However, the nanosheets lateral size and thickness were observed to be invariant with all production parameters, but the surfactant concentration. The authors reported that by adjusting the surfactant concentration the nanosheets lateral size can be controlled between ~40 and ~200 nm, while the thickness can be controlled between ~2 and ~12 layers. A clear dependence between the yield, zeta potential, thickness and lateral size of the nanosheets was observed with the surfactant concentration (C_{surf}), Fig. 5A–D. In details, as the surfactant concentration increases, so does the yield which saturates between C_{surf} values of 5–10 mg mL^{-1}, after which it begins to fall off rapidly at higher values of C_{surf}. The authors noted that this behaviour is distinct to that observed for graphene produced by shear-exfoliation, where the graphene concentration is known to depend on the ratio between surfactant and bulk concentrations, rather than C_{surf} alone. The dependence on the yield was explained by considering the CMC value of SC (~6 mg mL^{-1}). When this surfactant concentration is reached, the additional surfactant molecules form micelles rather than getting adsorbed onto the nanosheets, leading to a saturation of both yield and zeta potential. An increase in surfactant con-

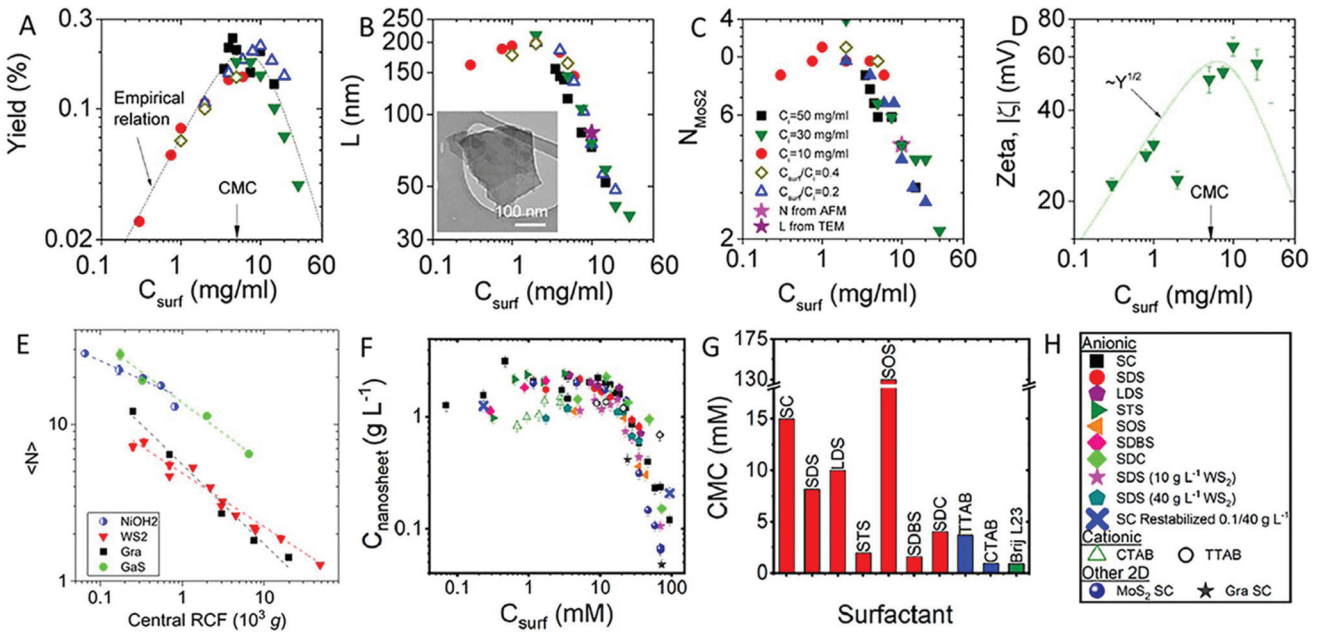

Fig. 5 (A) MoS_2 exfoliation yield, (B) nanosheet lateral size (L), (C) thickness as number of layers (N) and (D) zeta potential plotted *versus* aqueous SC concentration. (E) 2D nanosheets mean layer number plotted *vs.* centrifugal accelerations. (F) Different WS_2 nanosheet dispersions concentration as a function of surfactant concentration. The CMC value for each applied surfactant is show in (G). (H) Symbol legend for the used surfactant in (F). Reproduced from ref. 52, 89 and 118 with permission from the American Chemical Society.

centration is expected to destabilize the surfactant-coated nanosheets, leading to a decrease in the concentration. The dependence of C_{surf} on size and thickness of the nanosheets has been tentatively associated with the fact that the surfactant packing density at edges is probably different compared to that at the center of the nanosheets, making smaller flakes easier to stabilize compared to larger ones.[118] On the other hand, SC has been reported to lie flat on the surface of graphene with its hydroxyl and carboxyl groups orientated toward the aqueous solution,[120,121] hence further investigation is needed to clarify these results. After this initial work, SC became a popular surfactant choice for the LPE of TDMs and other 2D materials (see also Table 2).[52,89,122,123] For example, SC was selected to exfoliate and stabilize 6 different TMDs,[122] including MoS_2, $MoSe_2$, $MoTe_2$, WS_2, WSe_2 and WTe_2. This study found out that the exfoliated nanosheets have similar average lateral size (118, 113, 154, 104, 116 and 111 nm, respectively), hence they were exploited as catalysts for the hydrogen evolution reaction. It was found that the catalytic activity depends on the chemical composition as following: selenides > sulfides > tellurides.

In addition to SC, the LPE of TMDs with different types of surfactants has also been reported. For example, Mao *et al.* reported the use of sodium deoxycholate (SDC): bulk $MoTe_2$ and WTe_2 were added to aqueous SDC solution (10 mg mL^{-1}) and sonicated for 8 hours.[124] The smallest measured thicknesses were 3 nm and 2.5 nm for $MoTe_2$ and WTe_2, respectively. The lateral size of these TMDs did range from 500 nm to 2 μm, depending on the processing conditions. These suspensions were observed to be quite stable, and show no precipitation after storage in ambient conditions for one month. The dispersion was then dropped on side-polished fibers to test its non-linear saturable absorption properties. Another work used SC and SDC for preparation of MoS_2 dispersions.[125] Bulk MoS_2 was sonicated for 12 hours in aqueous SC or SDC solution (10 mg mL^{-1}), centrifuged at 4200*g* for 1 hour and the supernatant was then collected for further characterization. It was observed that the average lateral size of nanosheets produced in SC and SDC were similar, however SDC achieved a higher dispersion concentration (0.085 mg mL^{-1}) and contained larger, few layer nanosheets in comparison to SC. In addition to small-molecule surfactants, long alkyl chain surfactants have been also shown to be effective for dispersant-assisted LPE. Cetyltrimethylammonium bromide (CTAB) and sodium dodecyl sulfate (SDS) were used to investigate the role of the surfactant in the production of aqueous dispersions of MoS_2 by bath sonicarion.[126] After 8 hours sonication, the exfoliated dispersions were treated with a two steps centrifugation at 4000 and 7000 rpm and the resulting precipitate was then collected for characterization. The MoS_2 zeta potential was measured as +62 and −58 mV for CTAB and SDS dispersants, respectively. In the case of nanosheets obtained with CTAB, the thickness of the nanosheets was in a narrow range (1–1.5 nm): this suggests the nanosheets to be 1–2 layers thick, whereas the lateral size of the flakes was around 70–75 nm. This work is also one of the few studies reporting the use of advanced techniques to understand the adsorption of the dispersant onto the nanosheets. Solution-state nuclear magnetic resonance (NMR) technique, such as ^{1}H NMR, diffusion ordered spectroscopy (DOSY), and transfer nuclear Overhauser effect spectroscopy (tr-NOESY), were used to distinguish between free and adsorbed molecules on the nanosheets and to identify how the dispersant is assembled onto the nanosheet. From the results, the authors suggested that bound and free surfactant chains undergo rapid exchange, which makes difficult to distinguish the corresponding contribution by NMR. The NOESY NMR results suggest that the surfactant chains could be arranged randomly and flat on the basal-plane of the sheets, forming a monolayer: there are no specific sites to which the surfactant molecules are bound, but they remain attached to the surface by dispersive interactions between the alkyl chains of the surfactant and MoS_2 nanosheets. These interactions, being weak, allow the bound chains to undergo rapid exchange, detachment and reattachment, with free surfactant chains in the dispersion, by explaining the overall results obtained by NMR.[126] This group further investigated CTAB stabilization for aqueous MoS_2 by MD simulations and measuring zeta potential at different ionic strengths.[127] It should be highlighted that some studies have shown that different adsorption mechanisms were observed between facial and linear amphiphiles.[89,128] It is generally accepted that facial amphiphiles adsorb flat, side-by-side, on the surface of 2D nanosheets, providing better coverage of the 2D nanosheet surfaces.[121,128,129] The linear amphiphiles, on the other hand, are suggested to adsorb on the 2D nanosheets surface in different ways: some studies show that the alkyl chains assembled flat on the 2D nanosheet surface and other studies suggested formation of hemimicelles on the surface depending on the concentration of surfactant and/or the alkyl chain length. Moreover, as discussed before, surfactant molecules are subjected to rapid exchanges, providing partial shielding coverage of the surface of the 2D nanosheets.[120,126–128,130]

Several studies have been dedicated to the investigation of the size and thickness distributions of produced nanosheets and their relation with the fundamentals of LPE. In particular, one study has shown that narrow fractions containing nanosheets with different lateral dimensions and thicknesses, and even monolayer enriched fractions, can be isolated from the mother dispersion using liquid cascade centrifugation (LCC).[131] It was also observed that WS_2 nanosheets isolated in fractions of comparable thickness to graphene, were significantly smaller in lateral size (Fig. 5E). A study on the exact relationship between size and thickness of flakes has been presented by Backes *et al.*[52] where several TMDs (WS_2, MoS_2, $MoSe_2$, $PtSe_2$) were exfoliated by tip sonication in aqueous SC. It was observed that the average lateral size, width and layer number of nanosheets decrease as power laws, with increasing centrifugal acceleration in all cases, however the exact trend is material-class dependent *i.e.* different TMDs are similar, yet distinct to graphene. This observation has been explained by noting that the lateral size-thickness relationship is dependent on both the interlayer and intra-layer binding strength of the

material.[52] This conclusion is in agreement with Ji *et al.*,[132] who reported that a stronger intralayer but weaker interlayer binding strength can result in larger, thinner flakes and *vice versa*.

Since the exfoliation study reported in ref. 118, the CMC value has been considered as the optimal surfactant concentration to achieve the highest yield and concentration of nanosheets, for fixed processing parameters. However, recent studies[61,89] have initiated a discussion on the importance of the CMC value in the exfoliation of TMDs. Griffin *et al.*[89] exfoliated WS_2 in a large range of surfactants, using different surfactant concentrations, while using the same exfoliation and centrifugation conditions for each sample. SC, SDC, SDS, sodium tetradecyl sulfate (STS), sodium octyl sulfate (SOS), lithium dodecyl sulfate (LDS), SDBS, CTAB, and tetradecyltrimethylammonium bromide (TTAB) were investigated. Each sample was sonicated for 2 hours by tip sonication by using 4–16 different surfactant concentrations (0.03–30 mg mL^{-1}), covering a range of different concentrations, below and above their CMC value. When plotting the nanosheet concentration as a function of C_{surf}, all data collapsed onto the same curve, Fig. 5F–H, indicating that under the same processing conditions, the final concentration is not determined by the type and amount of surfactant, in agreement with previous works on graphene.[133] Below a C_{surf} value of 5 mg mL^{-1} of C_{surf}, the nanosheet concentration was roughly constant at 1–2 mg mL^{-1}; the concentration strongly decreases for increasing C_{surf}, no matter the CMC value of each surfactant. Hence, it was concluded that incorporation into micelles is not necessary to achieve efficient exfoliation with surfactants. In conclusion, ref. 89 has shown that no clear correlation between CMC or types of surfactants and exfoliation efficiency exists, in contrast to ref. 125 results, and in agreement with the observations from ref. 118. It is suggested that the dependence between dispersed concentration, lateral size and thickness observed may be related to a more general effect, possibly to electrostatic screening, although details are still under investigation. Another work from the same group also investigated the effect of the starting bulk material in SC-assisted LPE in water.[123] Dispersions starting from six different MoS_2 powders (7.5 mg mL^{-1}) were produced by tip sonication for 5 hours in aqueous SC (2 mg mL^{-1}). The resulting MoS_2 nanosheets were then analyzed based on quantitative spectroscopic metrics previously proposed in ref. 119. The results demonstrate that the effect of the different starting materials on exfoliation yield and size of the obtained nanosheets are negligible. However, it was also observed that monolayer MoS_2 exfoliated from the smaller bulk crystals exhibits weaker photoluminescence intensity.

Polymers, including synthetic and natural types, have been used as dispersants in LPE of TMDs in low boiling solvents. For example, in one study 9 polymers with various Hildebrand solubility parameters were investigated, including the synthetic polymers: s polybutadiene, poly(styrene-*co*-butadiene), polystyrene, poly(vinyl chloride), poly(vinyl acetate), polycarbonate, poly(methyl methacrylate) and poly(vinylidene chloride), natural polymer cellulose acetate (CA).[90] Various TMD powders (0.3 mg mL^{-1}) were added to polymer solutions (3 mg mL^{-1}) in tetrahydrofuran (THF) then tip sonicated for 0.5 hours. The resulting MoS_2 concentrations were in the range of 0.017–0.033 mg mL^{-1}. The resulting MoS_2 nanosheet dispersion concentration was in the range of 17–33 μg mL^{-1}. In a different work,[134] LPE of MoS_2 in ethanol was performed with PVP/ethanol. It was claimed that the use of the polymer allowed to achieve higher concentration, compared to the use of pure ethanol, although quantification was not provided. The MoS_2 nanosheets were reported to have an average thickness of around 3 nm. The material was then used for the fabrication of a non-volatile re-writable memory, by exploiting the PVP insulating nature that allows charge trapping and de-trapping. In a more recent study, PVP was also used as dispersant in water to test a new deposition method that allows to produce 3D crumpled nanosheets by using a rapid spray drying technique.[135] In this work MoS_2, WS_2 and h-BN were treated with tip sonication for 1 hour in 10 mg mL^{-1} PVP aqueous solution. The final dispersion concentrations were 0.17, 0.15 and 0.35 mg mL^{-1}, with a corresponding average nanosheet lateral size of about 500, 400 and 204 nm for MoS_2, WS_2 and h-BN, respectively. Their average layer number for the three different materials were in the range of 2–5.

One of the most common reasons for using a polymer as dispersant is related to the use of 2D materials as inclusions in composites. WS_2 was exfoliated in aqueous poly(vinyl alcohol) (PVA) solution by tip sonication for 1 hour.[136] After centrifugation, unexfoliated bulk was removed. Then, high and low rotation speeds were used to obtain dispersions with relatively small and large nanosheets. The monolayer yield in the two dispersions was around 6.1 and 3.1%, respectively. The mean lateral size for large nanosheets was 120 nm and for small nanosheets was 60 nm. The unique optical properties of WS_2 were exploited to study re-aggregation during drying, which is an important process in composite applications. The composites formed were shown to be readily dispersible in water leading to complete recovery of the spectral features. This feature was important as it allows the material to be recovered and re-used. Semiconducting polymers have been also investigated as dispersants, Table 2. The polymer poly(3-hexylthiophene) (P3HT), a semiconducting polymer widely studied for use in organic transistors and photovoltaics, has been exploited for dispersant-assisted LPE in chloroform by demonstrating a novel 2D organic/inorganic semiconductor hetero-junction, exhibiting reverse saturable absorption, in contrast to both pure P3HT and MoS_2.[137] This nonlinear optical feature is attributed to the charge transfer between the organic and inorganic material.

A detailed study into dispersant-assisted LPE by using non-ionic stabilizers (eight of which are polymers) was presented in a work from Guardia *et al.*[138] Various bulk TMDs (30 mg mL^{-1}) were added to 10 different aqueous solutions and sonicated for 5 hours. The highest MoS_2 concentration reported (~12 mg mL^{-1}) was obtained by using P-123-polyoxyethylenesorbitanmonooleate (P123), providing an exfoliation yield up to 40%. Note, however, that this exceptional concentration was obtained by using a very high surfactant concentration

(12 mg mL^{-1}). In general, only very few surfactants produced MoS_2 concentrations higher than the one obtained by mixed solvents, under the same experimental conditions. In the case of WS_2, the highest concentration was ~3 mg mL^{-1}, obtained by using *n*-dodecyl β-D-maltoside, a small-molecule surfactant, in high concentration (10 mg mL^{-1}). P123 also did show to provide high exfoliation yield, but only if used at very high concentrations. It is therefore unclear if a non-ionic surfactant could provide a good alternative to ionic surfactants, as the high residual amount may affect possible use of the material, hence re-processing is needed.[138] One has also to note that the presence of the polymers increases the viscosity of the medium (as function of their molecular weight), which has an impact on the sedimentation coefficient of the nanomaterial so that the high dispersed concentrations could partially be related to less efficient removal of "unexfoliated" material.

A systematic study on 19 different poloxamers used as stabilizers for exfoliation of TMD materials in water was reported by Mansukhani *et al.*[139] These biocompatible and non-ionic block copolymers can be used as dispersants due to their amphiphilic nature: they are made by a hydrophobic polypropylene oxide (PPO) chains and hydrophilic PEO chains in different lengths and ratios. Based on their structure, they are divided into two types: pluronic and tetronics. The PPO chains non-covalently adsorb to the surface of MoS_2 through hydrophobic interactions, while the hydrophilic PEO chains extend into solution by providing stabilization, Fig. 6A. The relative lengths of the PPO and PEO chains will influence these amphiphilic interactions and thus lead to variations in exfoliation and dispersion efficiency. Indeed, a wide range of concentrations were observed, despite using exactly the same processing parameters. Amongst all dispersants tested, Pluronic F87 yielded the maximum concentration of MoS_2 (0.12 mg mL^{-1}), demonstrating that pluronics with an intermediate PEO molecular weight are the most efficient dispersants for LPE of TMD materials, Fig. 6B. The average thickness and lateral size of the MoS_2 nanosheets was ~5 nm and ~28 nm respectively. In addition to MoS_2, other 2D materials including h-BN, WS_2, SnSe, $MoSe_2$ and WSe_2 were exfoliated with Pluronic F87 (see following sections), reaching concentrations in the range of 0.07–0.34 mg mL^{-1}. As these polymers are biocompatible, this approach is very attracting for biomedical applications,[140] while it may be more difficult to apply the exfoliated material in electronics, as these polymers act as electronic insulators or charge trap carriers, hence they can negatively affect the device performance. Another work[141] reported the use of two different triblock copolymers for exfoliation of MoS_2. Inspired by a study reporting that continuous addition of surfactant can improve graphene exfoliation yield,[142] the aqueous triblock copolymer solution was added continuously during MoS_2 exfoliation. The nanosheets concentration was observed to scale up with amount of surfactant and the more hydrophilic polymer showed better exfoliation yield. The average thickness was 1.5–2 nm and the lateral size was about 55 nm. Moreover, the MoS_2 dispersions remained stable for more than 6 months. Although high quality nanosheets were obtained, the concentration of MoS_2 nanosheet was much lower compared with the values obtained in ref. 138, possibly due to the different experimental conditions used. One of the advantages of using poloxamers is the ability to use them as exfoliating agents as well as to separate polydisperse 2D material dispersions based on buoyant density.[143] This approach is called: "density gradient ultracentrifugation" (DGU) and it has been applied successfully to many nanomaterials, from carbon nanotubes to graphene.[144–149] Kang and co-authors[143] chose Pluronic F68 (F68) to exfoliate and modify MoS_2. They calculated that the buoyant density of F68-functionalized MoS_2 will decrease to an acceptable range, in comparison with iodixanol, due to efficient hydration interactions of F68. The MoS_2 crystal was tip sonicated for 1 hour in 20 mg mL^{-1} aqueous F68 solution. After DGU size separation (Fig. 6C), selected fractions of the dispersion were characterized: the fractions corresponding to the top layers were on average thinner than those at the bottom. Hence, this is an efficient method for production of enriched dispersions of monolayer MoS_2.

Amongst natural polymers, CS has been used as a stabilizer in aqueous TMD dispersions (Table 2). CS was used to modify MoS_2 during exfoliation to enhance the nanocomposites flame retardance properties, and to provide better interaction with epoxy, allowing good dispersion of MoS_2 in this polymer.[150] The fabricated nanocomposites exhibited improved properties in heat-release rate and toxic volatiles release, compared to pure epoxy. The authors suggest that MoS_2 acts as a nanobarrier to combustible gas release, restraining toxic compounds effusion, by reducing fire hazards significantly. Another work[151] reports exfoliation in CS: in this case, this dispersant was selected because CS can be protonated to polycationic material in acid media,[152] which is expected to improve the interaction between the polymer chains and the MoS_2 nanosheets, based on previous results obtained from LPE of graphene. With this method, the maximum MoS_2 concentration was reported at 0.85 mg mL^{-1}, corresponding to about 25.5% exfoliation yield. In another study, CS was used to make MoS_2 dispersions suitable for theranostics.[153] Commercial MoS_2 flakes were ground with NaCl and treated with oleum at 90 °C under stirring. After removing oleum, the oleum-treated MoS_2 solution was sonicated and centrifuged to obtain a homogeneous and water-soluble black dispersion, which remained stable for at least 1 week. The average thickness of the nanosheets was in the range of 4–6 nm, which is larger than the expected value for MoS_2 single layer due to the presence of a CS coating. The average lateral size of the nanosheets was 80 nm. The zeta potential measurements indicate that the nanosheets were cationic at pH 6. The nanosheets were then used for near-infrared photothermal-triggered drug delivery for cancer therapy, for which MoS_2 is very attractive, due to its efficient photo-thermal conversion responsivity. The authors suggest that dispersant-assisted LPE is a very attractive alternative to the most used method of synthesis of MoS_2 dispersions for theranostics, which is based on lithium ion intercalation: this process is typically performed at high temperature and

makes use of *n*-butyllithium, which is hazardous.[154] For a comprehensive discussion of 2D materials used for theranostics we suggest the reader to look at recent reviews published elsewhere.[44,155]

Amongst biopolymers, cellulose and lignin, which have similar chemical structures of CS, were used as stabilizers for assisted LPE of MoS_2 (Table 2). In particular, nano fibrillated cellulose (NFC) has been used by Li *et al.*[156] for the production of MoS_2. NFC is a desirable polymer to use as it is green and environmentally friendly. A dispersion of MoS_2 was produced *via* sonication for 4 hours in an aqueous solution of NFC (2.5 mg mL^{-1}). A final concentration of 0.9 mg mL^{-1} was achieved with a yield of ~18%. The obtained dispersion had a zeta potential of −38.3 mV and was stable for more than 2 months. The nanosheets lateral size was reported to be in the range of 200 nm to few μm. The second-most naturally abundant biopolymer after cellulose is lignin. Alkali lignin (AL) was used for dispersant-assistant LPE of MoS_2.[157] With the addition of AL, the MoS_2 nanosheet concentrations were reported to achieve concentration up to 1.75 mg mL^{-1}, although a long exfoliation time was required (80 hours). The authors attribute dispersion stabilization to both electrostatic and steric effects. In the same work it was reported that AL can also exfoliate other 2D materials in water, including WS_2 and h-BN, although the concentrations were not very high. A few studies also reported the use of culinary aqueous gelatine,[158] gum Arabic,[138] guar gum and xanthan gum,[159] as dispersants in water. Furthermore, BSA has been successfully used for the LPE of MoS_2 in water, Fig. 6D.[160] The MoS_2 dispersions were produced by sonication for 48 hours and then subject to centrifugation. The resulting MoS_2 concentration was 1.36 mg mL^{-1} with an exfoliation yield of 27.2%. The dispersions obtained using BSA are very stable, even after storage for a year, and their high dispersability was not influenced by changes in pH from 0 to 14. It was estimated that there are ~120 BSA molecules on each nanosheet. In addition, the bound BSA can be partially removed by increasing the number of high speed centrifugation steps with water *via* centrifugal force, although this process will cause some re-aggregation of the MoS_2 nanosheets. It is proposed that after adding MoS_2 into BSA solution, BSA molecules are stably bound to the surface of MoS_2 crystals *via* the strong hydrophobic interaction, while polar groups of BSA are exposed externally in water. During sonication, the surface layer of MoS_2 crystals adsorbed with BSA can slide gradually and irreversibly as the freshly exposed surfaces are immediately covered by free BSA, leading to the exfoliation of bulk MoS_2 in water. The crystals showed a high average thickness of about 10 nm, which was attributed to BSA adsorbed on both sides of the nanosheets. The average lateral size of these MoS_2 nanosheets was around 100 nm. It was also noted that efficient exfoliation was achieved under sonication with low energy density by using a bath sonicator instead of a tip sonicator. Finally, the authors highlighted that BSA can efficiently exfoliate graphite into graphene as well as MoS_2, while other proteins, such as fibroin, do not perform well in the exfoliation of both materials. This shows the importance of selecting the dispersant by taking into account of the chemical structure of the 2D material: an efficient dispersant for exfoliation of graphene is not necessarily efficient at exfoliating other 2D materials and *vice versa*. Finally, single-stranded (ss)DNA was used as dispersant for WS_2 and WSe_2 exfoliation, Fig. 6E.[161] Bulk material (1.0 mg mL^{-1}) was added to aqueous (ss)DNA solution (1.5 mg mL^{-1}) then treated with tip sonication for 3 hours. After removing un-exfoliated crystals, the concentrations of WS_2 and WSe_2 were reported to be 0.87 and 0.81 mg mL^{-1}, respectively. The exfoliation yield reaches up to 87% for WS_2 and 81% for WSe_2. The exfoliation yield was observed to increase more than 20 times, compared the throughput without the (ss)DNA dispersant. The lateral size of the nanosheets was in the range of 60 to 650 nm with an average thickness below 10 nm for WS_2 and WSe_2 nanosheets. The anti-bacterial activity of WS_2 and WSe_2 against *Escherichia coli* K-12 MG1655 was then tested.

Amongst small organic molecules, pyrene derivatives have been shown to be an effective dispersant choice for the exfoliation of TMDs as well as for graphene in water, Table 2. Within our group, we have employed pyrene derivatives as exfoliating agents to produce dispersions of four different TMDs. Pyrene derivatives investigated include (Fig. 6F): PS1, 6,8-dihydroxy-1,3-pyrenedisulfonic acid disodium salt (Py2) and 1,3,6,8-pyrenetetrasulfonic acid tetrasodium salt (Py4).[101] Amongst all of them, Py2 was shown to achieve the highest exfoliation efficiency whereas Py4 is ineffective at exfoliating layer materials due to its high solubility in water. Our group further used PS1 as the exfoliating agent to obtain aqueous MoS_2, WS_2, $MoTe_2$ and $MoSe_2$ dispersions, which were used to print the photoactive element of in plane and vertical photodetectors.[43,162,163] Wu *et al.*[164] recently reported the exfoliation of MoS_2 with 1-pyrene-butyrate salts, including 1-pyrenebutyric acid sodium salt (PyB-Na) and 1-pyrenebutyric acid tetrabutylammonium salt (PyB-TBA). The exfoliation process is rather different from the traditional protocol as the MoS_2 powder was kept for 24 hours at room temperature (eventually under magnetic stirring) before sonication to facilitate the intercalation of the PyB molecules into the bulk material. Distilled water (270 mL) was added before shear mixing at 6000 rpm. The dispersions were kept still for 4 hours and the top 200 mL of the suspension was decanted and centrifuged. The as-exfoliated MoS_2 exhibited a high degree of crystallinity with an average nanoflakes thickness of 5 nm, and extremely large size (several μm), which is rather unusual. Similar results were obtained by Chen *et al.*[165] where organic salts such as imidazole or pyridiniumtribromide were used as dispersants. Concentration up to 4 mg mL^{-1} and nanosheets with average thickness of 0.9 nm were reported, also exhibiting extremely large lateral size (up to 50 μm). To improve the dispersion stability at different pH values, Chen *et al.*[166] reported the use of *p*-phosphonic acid calix[8]arene. The as-synthesized dispersions of graphene, h-BN, MoS_2 and WS_2 dispersions had a pH value of about 3, with zeta potential of −68 mV, −63 mV, −50 mV, −50 mV, respectively. When the pH value of the dispersions was adjusted between 2–12, the dispersions showed

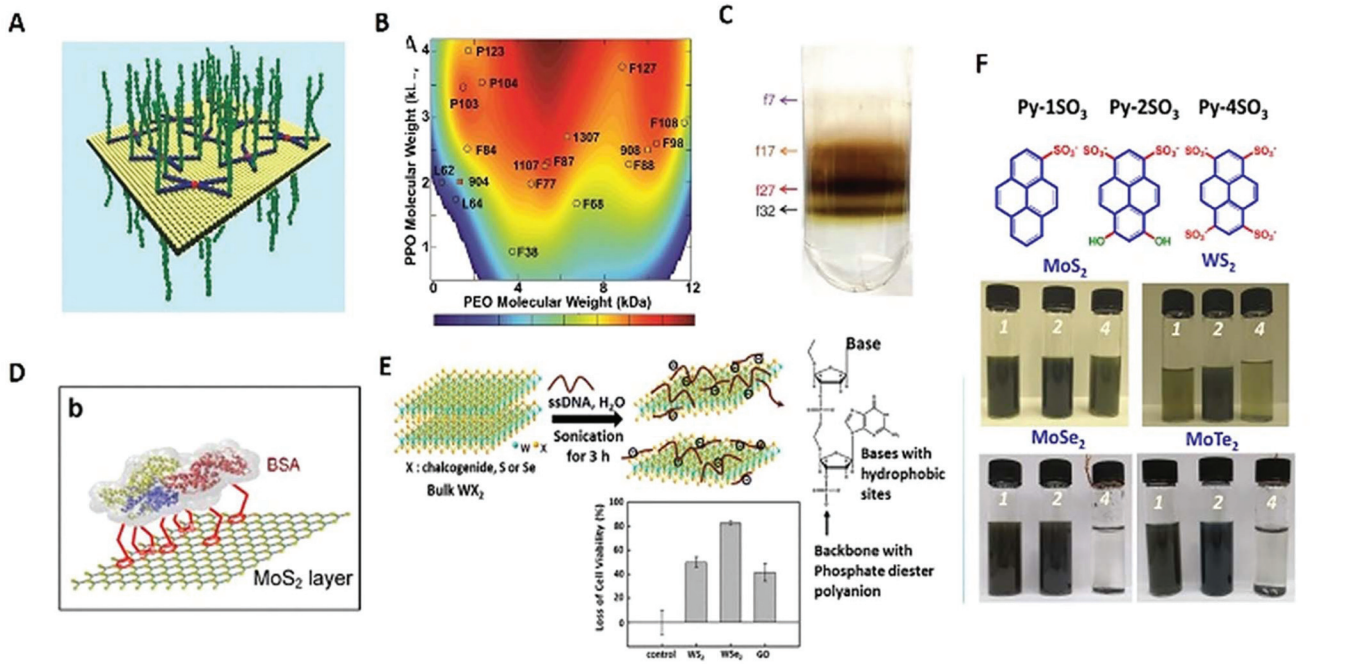

Fig. 6 (A) Schematic for monolayer MoS_2 with tetronic block copolymers absorbed on the surface. (B) MoS_2 concentration map in pluronics and tetronics. (C) Digital picture of a tube with MoS_2 bands after the first iteration of DGU. (D) Schematic diagram of BSA binding with single-layer MoS_2 layer binding. (E) Schematic for ssDNA assisted WS_2 and WSe_2 LPE process. Right: ssDNA backbone structure with phosphate diester polyanion. Bottom: Antibacterial activity comparison of exfoliated WS_2-ssDNA, WSe_2-ssDNA and graphene oxide nanosheets against *Escherichia coli* K-12 MG1655 cells. (F) Four different TMDs exfoliated dispersions with pyrene derivatives. In the digital images 1, 2 and 4 responding to the added molecule are Py-1SO_3 (PS1), Py-2SO_3 (Py2) and Py-4SO_3 (Py4). Reproduced from ref. 101, 139, 143, 160 and 161 with permission from IOP Publishing, Wiley-VCH, Springer Nature and the American Chemical Society.

good stability as their zeta potential kept in the range of −50 to −80 mV. Other organic molecules used as dispersants include: tannic acid,[159] hyaluronic-functionalized pyrene,[167] alkylamine[168] and thioglycolic acid, which can be used as dispersant due to its thiol interaction with MoS_2, while its COOH functional group allows dispersion and stabilization in water.[169] Finally, amongst small biomolecules, Ayan-Varela *et al.*[170] have shown that MoS_2 can be exfoliated in deoxyadenosine monophosphate (dAMP) and deoxyguanosine monophosphate (dGMP), reaching relatively high concentrations (1.7–1.8 mg mL^{-1}), while exfoliation was not very effective with others types of nucleotides. This result was attributed to the higher basicity for dAMP and dGMP, which allows better adsorption onto the TMDs *via* acid–base interaction, compared to the π–π interaction with graphene.

We remark that only a very few works have been dedicated to less famous TMDs, such as TiS_2 and ReS_2. In the case of TiS_2, one of the major problems is related to its reactivity to water or oxygen.[171] As we will show later, the stability of air-sensitive materials is usually improved by LPE, in particular after adsorption of surfactants. However, a recent study[172] has shown that TiS_2 nanosheets, obtained from tip sonication in aqueous SC solution (2 mg mL^{-1}) at a starting concentration of 20 mg mL^{-1}, oxidized almost completely within hours. In contrast, ReS_2 is well-known for its stability in air and water. Hence, this crystal can be exfoliated in water using traditional surfactants as stabilizers. Kang *et al.*[173] successfully exfoliated ReS_2 powder *via* ultrasonication in aqueous SC solution. The resulting dispersion was then centrifuged at 7500 rpm to remove unexfoliated ReS_2 powder and then further ultracentrifuged at 20 000 rpm to collect nanosheets with relatively large lateral sizes. DGU was also performed by using caesium chloride, demonstrating sorting by thickness.

3.2 Hexagonal-boron nitride

Bulk h-BN consists of an equal number of B atoms and N atoms arranged alternately to form a hexagonal structure. In the h-BN monolayer, B and N atoms are covalently bonded, and the distance between adjacent atoms in-plane is 2.504 Å. The h-BN monolayers are stacked by van der Waals forces, and the inter-plane distance is about 3.30 Å. Bulk h-BN, the so-called "white graphite", is a structural analogue of graphite. Its attractive properties include: a wide band gap (5.7 eV) over a wide range of energies, higher chemical inertness, thermal stability, and resistance to oxidation. LPE of h-BN was reported first in ref. 29, 174 and 175. using organic solvents, although exfoliation of h-BN in water is also possible, but at lower concentration.[74]

Dispersant assisted LPE of h-BN has been widely used (Table 2): the use of SC and SDC allows production of h-BN dispersions with concentrations up to 2.37 and 1.67 mg mL^{-1}, respectively, which are significantly higher than the concen-

tration obtained without surfactant (0.1 mg mL^{-1}).[176] The authors claimed that sonication treatment can turn h-BN into h-BN-OH due to hydrolysis in aqueous solution, by improving exfoliation. While h-BN-OH still maintains a hydrophobic and π rich basal plane, the σ-bonding rich SC and SDC can interact with h-BN-OH *via* σ–π interactions. Therefore SC and SDC addition has been shown to improve h-BN exfoliation and stability, as compared to exfoliation in water only.[176] SC assisted LPE of h-BN was also demonstrated by other groups,[52,117,118,138] although the concentrations of h-BN nanosheets reported is much lower than 1 mg mL^{-1}. The difference in h-BN nanosheet concentrations may come from the use of different bulk material concentrations and other processing parameters.

The first work reporting use of a polymer for LPE of h-BN has been reported by Han *et al.*:[174] 0.2 mg of h-BN crystals was added in a 5 mL 1,2-dichloroethane solution of poly(*m*-phenylenevinylene-*co*-2,5-dictoxy-*p*-phenylenevinylene) (0.12 mg mL^{-1}) to sonicate for 1 h. Characterization by transmission electron microscopy confirmed exfoliation down to few- and single-layer nanosheets, Fig. 7A. The amphiphilic copolymer F68 was also used in h-BN exfoliation and size sorting.[177] Bulk h-BN was tip sonicated for 2 hours in aqueous F68 solution (20 mg mL^{-1}) at a concentration of 40 mg mL^{-1}. After three steps of DGU treatment, monodispersed h-BN nanosheet fractions could be obtained (Fig. 7B). The smallest nanosheet thickness was 0.73 ± 0.11 nm, while other nanosheets fractions had thickness in the range of 2–8 layers. In this work, LPE of h-BN in SC was also performed for comparison. The authors observed that SC had weaker ability to sort thicker h-BN due to its smaller surface packing density and equivalent anhydrous shell thickness on h-BN, as compared to results observed in case of graphene exfoliation.[177]

PVP, already widely used as dispersant for LPE of many 2D materials, has been used also for h-BN exfoliation (Table 2): Bari *et al.*[135] reported dispersion concentrations up to 0.35 mg mL^{-1} by sonication of h-BN in aqueous PVP solution (10 mg mL^{-1}) for 1 hour. The lateral size of the nanosheets was about 204 nm, while their average thickness was around 2–5 layers. May *et al.*[90] undertook a similar systematic study performed on TMDs, in which different polymers were used for dispersant-assisted LPE: the bulk h-BN crystals (0.3 mg mL^{-1}) were tip sonicated in polymer and THF solution (3 mg mL^{-1}) for 0.5 hours. The obtained dispersion concentrations were rather low (2–34 μg mL^{-1}), this result was attributed to unsuitable Hildebrand solubility parameters between solvent and h-BN.[90] Another work reports the use of 19 non-ionic copolymers as dispersants for assisted-LPE of TMDs and h-BN.[139] These copolymers are poloxamers consisting of amphiphilic pluronics and tetronics in different ratios. Bulk h-BN in aqueous Pluronic F87 solution (10 mg mL^{-1}) was tip sonicated for 1 hour, achieving a final dispersion concentration of about 0.07 mg mL^{-1} which was significantly lower than achieved for the MoS_2 dispersion. The average flake thickness and lateral size were reported as ~4.5 nm and ~77 nm, respectively.[139] A study investigated the use of 8 different non-ionic polymers as well as SC as dispersants. Remarkably, the concentrations reported were all low (in the range of 0.046–0.18 mg mL^{-1}), which were even lower than the ones obtained by LPE without dispersants.[138] This was attributed to the functionalization of h-BN with hydroxyl groups during sonication in water, which would decrease adsorption of the dispersant's hydrophobic moieties onto h-BN. In addition to synthetic polymers, biopolymers have been used to achieve effective LPE of h-BN: for example, Biscarat *et al.*[178] reported the fabrication of gelatine/h-BN nanocomposites by a simple gelatine assisted LPE. Another group used gelatine as a dispersant, by obtaining a high h-BN concentration (1.4 mg mL^{-1}).[158] This dispersion was made by sonicating h-BN crystals (50 mg mL^{-1}) for 8 hours in 20 mg mL^{-1} aqueous gelatine solution. Besides gelatine, the biopolymers AL[157] and NFC[156] also showed good potential for the exfoliation of h-BN.[156] In the latter case, a zeta potential of −41.9 mV and lateral size from 200 nm to micrometres were reported. The authors observed that the h-BN dispersions have better stability compared to the h-BN dispersions obtained without NFC: after sitting for 10 days, aggregates appeared in the BN dispersion without NFC, while NFC-assisted dispersed BN solution kept stable (Fig. 7C).[156]

Our group has used pyrene derivatives to successfully exfoliate h-BN.[43,101,179] One of the most successful stabilizer in this family is Py2, which allowed to achieve 18.1% exfoliation yield and dispersions concentration of 0.544 mg mL^{-1}. PS1 dispersant assisted such h-BN nanosheet dispersions were applied as dielectrics in printed electronics.[101,179] In addition to polyaromatic dispersants, other small organic molecules like *p*-phosphonic acid calix[8]arene[166] and pyrene-conjugated hyaluronan,[167] were also used for assisted-LPE, by achieving dispersion concentrations of 0.1 and 0.6 mg mL^{-1}, respectively.

3.3 Black phosphorous

BP is an elemental crystal with a layered structure similar to graphite. The BP monolayer, called phosphorene, contains two sublayers, in which the valence orbitals of the P atom are sp^3 hybridized forming 3 covalent bonds with surrounding p atoms, whereas one lone pair of electrons occupy the final hybrid orbital. The BP monolayers are stacked with a pitch of 5.4 Å and held together by van der Waals forces.[180] Research on BP is increasing significantly, since few-layer BP has been reported to exhibit outstanding charge-carrier mobility and layer-dependent direct bandgap, unlike graphene.[181] Moreover, a large on/off ratio observed in transistors and highly anisotropic properties make few-layer BP a desirable candidate for applications within optoelectronics, energy storage and many others.[14] However, monolayer and few-layer BP nanosheets are sensitive to oxygen and moisture.[182,183] Despite this, successful LPE of BP has been reported with improved stability in air, due to solvent adsorption.[184] High-boiling-point solvents including NMP, DMF, DMSO, and *N*-cyclohexyl-2-pyrrolidone allow exfoliation of the bulk crystals and at the same time they help minimizing chemical degradation from ambient oxygen and water as they act as barrier between the nanosheets and the environment.[184–187] Aqueous

BP dispersions were successfully obtained by LPE by using SDS dissolved in deoxygenated water, prepared by purging deionized water with ultrahigh-purity Ar gas in a sealed container. Bulk BP was added in aqueous SDS solution (20 mg mL^{-1}) and sonicated for 1 hour. After centrifugation to remove the unexfoliated bulk material, the dispersion showed a concentration of 0.13 mg mL^{-1} and was composed by nanosheets with average thickness of about 4.5 nm. Compared with NMP-exfoliated BP dispersion, a higher concentration and narrow thickness distribution were observed (Fig. 8A and B). The zeta potential was about −70 mV, which was more negative than SDS-water (−55 mV) and BP in water (0 mV), showing improved dispersion stability. Microscopic and spectroscopic analysis showed that individual BP nanosheets possess properties comparable to micromechanically exfoliated BP flakes with no effects from chemical degradation following aqueous processing.[188] In a more recent work[189] bulk BP was added in aqueous SC solution (5 mg mL^{-1}), after shear exfoliation was applied by using a kitchen blender for 2 hours; the average thickness was ~19.1 nm, while the lateral size was in the range of 100–700 nm. The obtained BP nanosheets were further non-covalently modified with anthraquinone, showing improved chemical stability.[189] Recently, Kim *et al.* reported effective exfoliation and stabilization of BP in the presence of strongly interacting surfactants such as CTAB and tetrabutylammonium hydroxide (TBAOH).[190] Benefiting from ionic groups, these dispersants can interact with the lone pair electrons of BP. In this study, the bulk BP (0.1 mg mL^{-1}) was tip sonicated for 4 hours in aqueous CTAB and TBAOH solutions, respectively, at different concentrations. The thickness of the nanosheets obtained by CTAB-BP and TBAOH-BP was 3–10 nm, and above 20 nm, respectively. The nanosheet lateral size was in the range of 800 to 3000 nm for CTAB-BP and 500 to 1500 nm for TBAOH-BP. The zeta potential of the CTAB-BP dispersion was +50.93 mV and −45 mV for TBAOH-BP dispersion. In this work, DOSY and 2D NOESY spectroscopy were employed suggesting the interdigitated arrangement of surfactants on few-layer BP. Stability studies of CTAB-BP nanosheets show that the degradation is slower when exposed to ambient condition: only tiny oxidized bubbles are visible after 15 days. This has been attributed to the CTAB interactions with the nanosheets, which are stronger that those of TBAOH. Indeed, the TBAOH-BP nanosheets show significant oxidation after 5 days storage in ambient conditions.[190]

In addition to small-molecule surfactants, macromolecules have also been used: PVP was used to achieve a remarkable monolayer yield of up to 51%.[191] Bulk BP was added in PVP ethanol solution (0.2 mg mL^{-1}) at a concentration of 1 mg mL^{-1} and sonicated for 3 hours. The thickness of the obtained BP nanosheets was 0.6–0.8 nm, while the mean lateral size and width were about 658 nm and 264 nm, respectively. Absorption spectroscopy was used to demonstrate that about 90% of the nanosheets are stable over 20 days. No signs of apparent degradation (*e.g.* bubble formation) were observed even after exposure to ambient conditions for 24 hours.[191] Another work used PVP as an agent to produce few-layer BP dispersions in water.[192] In this work, bulk BP was sonicated in aqueous PVP solution (0.5 mg mL^{-1}) at a concentration of 2 mg mL^{-1} for 20 hours, then centrifugation was applied to remove unexfoliated bulk. This approach was observed to provide a much higher throughput yield (33.4%), compared to that of BP exfoliated in pure water (6.2%). The authors claim that this yield enhancement is related to the interaction with the pyrrolidinone group of PVP.[192]

Monomer ionic liquids have been demonstrated to efficiently exfoliate BP as well as to improve few-layer BP dispersions stability.[193–195] However, ionic liquids are typically expensive compared to traditional solvents used in LPE. A more economical approach is based on using a diluted polymer ionic liquid (PIL) into a solvent, as reported by Hu *et al.*[196] Imidazole-based PILs were selected and named as P([VPIm]Br), P([VPIm]PF_6) and

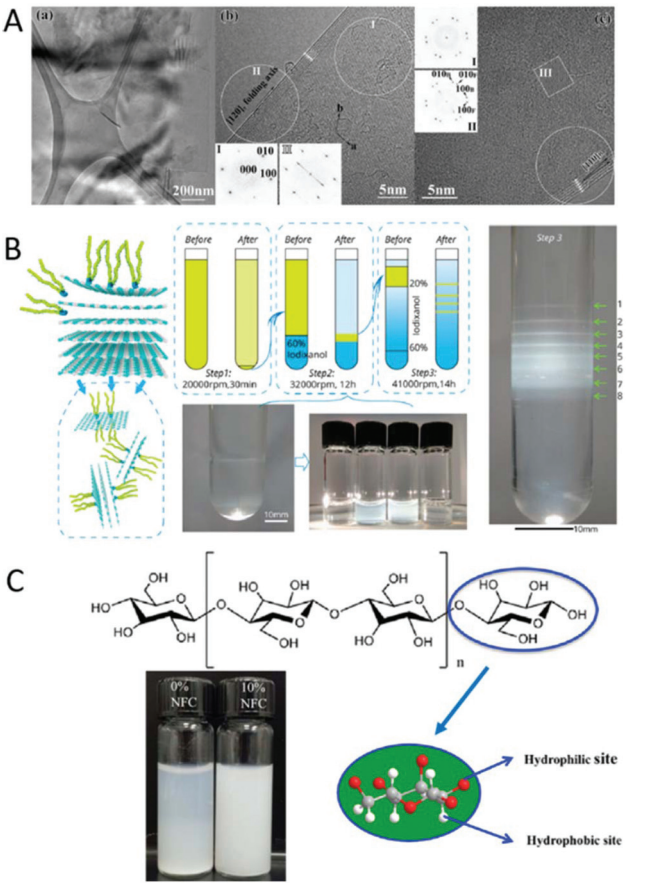

Fig. 7 (A) Low and high magnification transmission electron microscope (TEM) images of h-BN nanosheets. (B) Procedures for size sorting of exfoliated h-BN by DGU. Left: Schematic diagram of the h-BN LPE process with F68. Middle top: Three operation steps for this DGU illustration. Middle bottom left: A photograph after step 2. Middle bottom right: Four vials with solution fracted from the right vial. Left: A photograph after step 3 effective exhibiting distinct 8 bands. (C) Hydrophilic and hydrophobic sites of glucose and a photo of h-BN dispersions with and without nanofibrillated cellulose addition after sitting for 10 days. Reproduced from ref. 156, 174 and 177 with permission from the American Institute of Physics, the American Chemical Society and Elsevier.

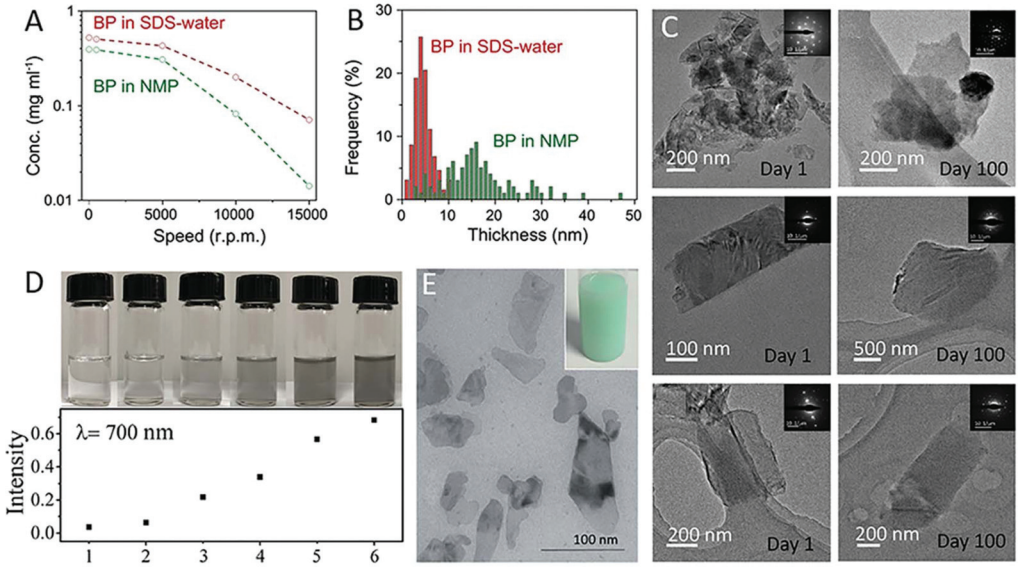

Fig. 8 (A) BP concentration as a function of the centrifugal speed and (B) thickness distribution comparison between BP exfoliated in SDS-water and NMP. (C) PILs-modified PB nanosheet stability for 100 d with TEM monitor. (D) Digital images and absorption intensity of an antimony crystal exfoliated in different systems, 1 to 6 stand for DMF, isopropyl alcohol (IPA), IPA : water (4 : 1), 2-butanol, DMF + P([VPIm]TFSI) and DMF + P([VPIm]PF_6), respectively. (E) TEM image of $Ni(OH)_2$ nanoflakes. Inset: a photo of $Ni(OH)_2$ dispersion. Reproduced from ref. 188, 196, 202 and 205 with permission from United States National Academy of Sciences, Wiley-VCH and Royal Society of Chemistry.

P([VPIm]TFSI). Among them, P([VPIm]TFSI) showed the best exfoliation efficiency. Bulk BP (1 mg mL^{-1}) was added in P([VPIm]TFSI) DMF solution (7.61 mg mL^{-1}) and sonicated for 6 hours. The BP nanosheet dispersion showed a concentration of 0.19 mg mL^{-1} corresponding to 19% exfoliation yield. The nanosheets had thickness in the range of 1.6–4.9 nm. Moreover, the nanosheets were reported to be stable for more than 100 days under ambient conditions (Fig. 8C). The authors demonstrated that the PILs imidazole rings can interact with BP *via* electrostatic interaction and prevent water and oxygen to get in direct contact with BP, therefore improving the BP exfoliation yield and stability. Furthermore, the imidazolium rings can quench the free radical species during irradiation. Benefiting from PILs good ionic conductivity and high mechanical strength, the stabilized BP/P([VPIm]TFSI) exhibited good performance when used in a flexible photodetector.[196] In addition to macromolecules, the same group also utilized phytic acid as dispersant.[197] The BP crystals were added in phytic acid and DMF solution (4 mg mL^{-1}) and sonicated for 8 hours. After removing unexfoliated BP crystal by centrifugation, the nanosheets average thickness was 3–4 nm. With phytic acid addition, the obtained BP nanosheets were observed to have large lateral size: up to 24–28 μm in length and 4–6 μm in width.[197] Finally, tannin was exploited as dispersant for assisted-LPE with the goal to improve the stability of BP nanosheets in ambient conditions.[198] The material was shown to be stable after exposure to air for at least 10 days.

3.4 Other 2D materials

To the best of our knowledge, dispersant assisted LPE was reported only on a few types of less studied 2D materials: antimonene, the family of layered hydroxides and other layered materials found in nature.

Antimonene is considered as a promising candidate for future electronics, as it belongs to the same group of BP, hence it is characterized by a high carrier mobility and layer-dependent bandgap (0–2.28 eV), Fig. 1.[199–201] Xiao *et al.* utilized diluted PILs, including P([VPIm]PF_6) and P([VPIm]TFSI), to exfoliate antimony efficiently.[202] Bulk antimony was added at a concentration of 1 mg mL^{-1} in PIL dissolved in DMF and sonicated. After centrifugation, the resulting antimonene dispersions featured a concentration more than 10 times higher than achieved with the solvent alone (Fig. 8D). The maximum concentration reported by using the solvent alone for exfoliation was 0.2 mg mL^{-1}, whereas by adding P([VPlm]PF_6) into the solvent, a concentration of 16.26 mg mL^{-1} was achieved with an exfoliation yield of more than 20%.[202]

Layered hydroxides are composed by positively charged metal layers and compensating anionic interlayers. They are widely used as catalysts, bioactive nanocomposites and photoelectric active materials.[203] Amongst the members of this family, cobalt hydroxide has been exfoliated into $Co(OH)_2$ nanosheet with assisted LPE.[204] The bulk powder (20 mg mL^{-1}) was sonicated in aqueous solution of SC (9 mg mL^{-1}) for 4 hours. The dispersion was then centrifuged at 1500 rpm, 240*g* for 2 hours to discard the unexfoliated bulk. The nanosheets have lateral size between 20 to 300 nm, and about 88 nm on average. AFM showed that the dispersion is composed by 2 to 10 layers with a mean thickness of 6 layers, and mean lateral size of around 94 nm. Another member of the same family is the neutral transition metal hydroxides Ni$(OH)_2$, which is attractive because of its catalytic properties. In

Table 2 Summary of the works reporting dispersant-assisted LPE of TMDs, h-BN, BP and less studied 2D materials. We have selected works reporting details of both exfoliation and characterization of the nanosheets

					Thickness			
Dispersant/solvent	2DM	C_{disp} (mg mL^{-1})	C_{2d} (mg mL^{-1})	Yield (%)	nm	N	Lateral size (nm)	Ref.
SC/water	MoS_2	1.5	0.5	0.1	—	2–9	280	117
	MoS_2	10	0.5	1	—	2–12	40–200	118
	MoS_2	2–5	1.9–2	9.5–10	—	14–15	175–195	89
	WS_2	2–5	1.3–2	6.5–10		10.5–17	190–195	
	MoS_2	2	0.15	2	—	7	120	123
	MoS_2	10	0.05	0.51	9.5–9.7	—	87–89	125
	h-BN	5	2.37	19.75	<2	—	—	176
	BP	5	—	—	9.4–28.8	—	100–700	189
	$Ni(OH)_2$	9	0.6	3	10.2–11	—	122–130	205
SDC/water	MoS_2	10	0.09	0.85	7.7–7.9	—	89–91	125
	WS_2	2–5	1.5–2.2	7.5–11	—	11–12	190–195	89
	h-BN	5	1.67	13.92	>4	—	—	176
CTAB/water	MoS_2	10	—	—	1–1.5	1–2	70–75	126 and 127
	WS_2	0.3–1	1–1.5	5–7.5	—	15.5–21	210–230	89
	BP	1.46	—	—	3–10	—	800–3000	190
SDS/water	WS_2	0.5–1.4	1.7–1.8	8.5–9		11–15.1	195–205	89
	BP	20	0.13	13	4.5	—	—	188
STS/water	WS_2	0.1–1	0.9–2.5	4.5–12.5	—	12–14	195–205	89
SOS/water	WS_2	1–5	0.9–1.1	4.5–5.5		9.5–16.5	195–215	
LDS/water	WS_2	1–2.5	1.9–2.2	9.5–11		11.5–18	195–220	
TTAB/water	WS_2	2–4	1.2–1.3	6–6.5		13.5–14	200–205	
SDBS/water	WS_2	0.1–0.6	1.1–2.1	5.5–10.5		10.5–12	190–205	
TBAOH/water	BP	1.04	—	—	>20	—	500–1500	190
PVP/water	MoS_2	10	0.17	0.85	—	2–5	500	135
	WS_2	10	0.15	0.75		2–5	400	
	h-BN	10	0.35	1.75		2–5	204	
	BP	0.5	0.13	33.4	2.0–3.0	—	—	192
PVP/ethanol	BP	0.2	—	—	—	0.6–0.8	658 (length) 264 (width)	191
PVA/water	WS_2	2	0.42	1.4	6.1 (large) 3.1 (small)	—	120 (large) 60 (small)	136
Brij L23/water	WS_2	0.96–108	1.1–1.45	5.5–7.25	—	16–18	213–220	89
F127/water	MoS_2	100	0.13	1.3	1.5–2	—	55	141
TWEEN20/water	WS_2	0.36–48	0.3–2.1	1.5–10.5	15–16	—	200–215	89
TWEEN80/water	WS_2	0.39–11	0.3–2.2	1.5–11	15–16		213–220	
TWEEN80/water	MoS_2	6	1.2–1.8	4–6	6.45	—	—	138
	WS_2	6	0.3–1.3	1–4.3	7.21			
	h-BN	6	0.07–0.09	0.23–0.3	7.62			
F87/water	MoS_2	20	0.12	0.32	4.1–6.3	—	12–43.2	139
	WS_2	20	0.09–0.13	0.24–0.35	3.4–6.2		38.8–80	
	SnSe	20	0.06–0.08	0.16–0.21	3.5–9.3		23.3–117.5	
	$MoSe_2$	20	0.29–0.39	0.77–1.04	2.8–4.8		23.8–65.4	
	WSe_2	20	0.26–0.32	0.69–0.85	3.4–5.2		24.7–54.9	
	h-BN	20	0.06–0.08	0.16–0.21	2.4–6.6		39.1–114.9	
F68/water	MoS_2	20	—	—	3–153	—	10–407	140
	WS_2	20			2–221		12–384	
	WSe_2	20			2–202		14–304	
	$MoSe_2$	20			2–160		16–232	
	MoS_2	20	1.71	17.1	0.6–5	—	—	143
	h-BN	20	—	—	0.62–0.84 (smallest)	2–8	—	191
P([VPIm]TFSI)/DMF	BP	7.61	0.19	19	1.6–4.9	—	—	196
P([VPIm]PF_6)/DMF	Sb	16.26	0.2	20	2.2–5.1	—	—	202
CS/water	MoS_2	0.17	0.93	0.62	4–6	—	80	153
NFC/water	MoS_2	2.5	0.9	18	—	—	200–few μm	156
	h-BN	0.5	1.1	22			200–few μm	
AL/water	MoS_2	1	1.65–1.83	16.5–18.3	—	Few layers	100–500	157
	WS_2	0.5	0.16–0.22	3.2–4.4		Few layers	285.2	
	h-BN	0.5	0.09–0.13	1.8–2.6		Few layers	530.5	
Gelatin/water	MoS_2	20	0.8	1.6	2.21	—	—	158
	WS_2	20	0.9	1.8	2.17			
	h-BN	20	1.4	2.8	2.09			
Guar gum/water	MoS_2	10	0.24	1.2	—	3–6	20–300	159
BSA/water	MoS_2	1	1.36	27.2	10.65	—	100	160
(ss)DNA/water	WS_2	1.5	0.87	87	1.4–2.6	—	65–650	161
	WSe_2	1.5	0.81	81	<10		64–550	

Table 2 *(Contd.)*

Dispersant/solvent	2DM	C_{disp} (mg mL^{-1})	C_{2d} (mg mL^{-1})	Yield (%)	Thickness		Lateral size (nm)	Ref.
					nm	N		
PS1/water	MoS_2	0.1	0.036	1.2	—	5–7 av.	400–700	43 and 101
	WS_2	0.1	0.04	1.3		5–7 av.	100–800	
	$MoSe_2$	0.1	1.1	36.7		5–7 av.	—	
	$MoTe_2$	0.1	0.8	26.7		5–7 av.	—	
	h-BN	0.1	0.113 (pH = 2)	3.7		<6	400–1000	
	h-BN	1	—	—	2.4	—	100–150	179
PyB-Na/water	MoS_2	—	0.3	2	3.5–7	—	1000–3000	164
Imidazole/water	MoS_2	20	4	40	0.9	—	10 000	165
PC8/water	MoS_2	1	0.15	3	5	—	187.5	166
	WS_2	1	0.13	2.6	5		108.5	
	h-BN	1	0.10	5	4		295.0	
TA/water	MoS_2	5	0.15	1.5	—	3–5	20–300	159
Py-HA/water	MoS_2	1	0.36	12	16	—	—	167
	h-BN	1	0.6	20	12.5			
Thioglycolic acid/water	MoS_2	93	3.49	0.87	1	—	100–500	169
dAMP/water	MoS_2	1	1.7	—	—	10	260–265	170
Phytic acid/DMF	BP	4	—	—	3–4		24 000–28 000	197

Acronym definitions: tetradecyltrimethylammonium bromide (TTAB); polyoxyethylene (23) lauryl ether (Brij L23); triblock copolymers F127 (F127); polyoxyethylene (20) sorbitan monooleate (TWEEN 80); polysorbate 20 sorbitan monolaurate (TWEEN20); tannic acid (TA); pyrene-conjugated hyaluronan (Py-HA).

one study, $Ni(OH)_2$ was exfoliated in water using SC (Fig. 8E).[205] The pre-treated bulk $Ni(OH)_2$ was tip sonicated for 4 hours in aqueous SC solution (9 mg mL^{-1}) and then the unexfoliated materials were removed by centrifugation. The obtained dispersion had concentration of 0.6 mg mL^{-1}, while the nanosheets have average thickness of around 10 nm and lateral size of about 126 nm. The same methodology was applied to another two hydroxides: $Mg(OH)_2$ and $Cu(OH)_2$.[206]

Assisted-LPE in aqueous SC solution was also extended to layered materials easily found in nature, with differing purity and composition. Harvey *et al.*[207] successfully exfoliated talcum powder, cat litter and beach sand, which contain layered talc, silicate and clay respectively. The resulting dispersions contained high concentrations of talc, a bentonite/palygorskite mixture and mica nanosheets for the three starting materials respectively.

4 Summary and outlook

Following the extensive investigation of dispersant-assisted exfoliation of graphene in water, efforts have been made for applying the same approach to a wide range of 2D materials. Various types of dispersants have been studied, showing no detrimental effect on the structure of the nanosheets and the ability to control their surface chemistry and charge. Table 2 provides a summary of the works that have been discussed in this review. However, we want to point out that comparisons should be made carefully: LPE is a very versatile method, where many different parameters can be changed (sonication type, sonication power, sonication time, size of bulk crystal, *etc.*), which are not always reported in the manuscripts. In addition, a wide range of pre- and post-processing techniques are applied in combination with LPE, which can significantly change the nanosheets properties (size, thickness, amount, *etc.*). Often the full conditions used for the exfoliation are not even provided by the authors. For example, the centrifugation rate is often given in rpm, without reporting the g factor of the centrifuge, by making it impossible to reproduce the experimental results and to make a direct comparison between works performed by different groups in the majority of cases. Furthermore, a unified method to determine concentration is currently lacking. Typically, the concentration is either determined by the dry mass after filtration of a given dispersion volume, or *via* calculations from UV-Vis spectral data, which requires the absorption coefficient of the material to be known. In this second case, a further problem arises with the use of the absorption coefficient, whose exact value is reported to change with the size and thickness of nanosheets and therefore with different processing parameters.[56] Typically, the average coefficient for each material is used, however this is not necessarily the correct value to use unless the experimental conditions used are closely matching with those from which the average coefficient was derived. In addition, the derivation and use of the absorption coefficient is still under discussion, but in many studies this factor is not considered when discussing the final dispersion concentration. Furthermore, some works report absorption measurements using an integrating sphere, to isolate the effects of light scattering, whereas others use standard UV-Vis spectrometers thereby measuring the extinction spectra.[56] In addition to the concentration, there are also inherent issues with the characterization of the size and thickness of nanoflakes produced by dispersant-assisted LPE, therefore the results obtained may not be directly comparable: first, if the range of lateral sizes or thicknesses of nanoflakes are considered, it should be noted that the both the upper and

lower limits will be affected by the centrifugation steps used. Second, in the case of dispersant-assisted LPE, thickness measurements are particularly challenging: the adsorption of molecules can change significantly the measured thickness of a single-layer, as molecules are adsorbed on both sides, and possibly in a disordered arrangement. Hence, it is challenging to turn measurements of thickness taken in nm into number of layers. The measured thickness will also depend on the amount of free dispersant in solution, as this will get deposited on the nanosheets upon evaporation of the solvent during sample preparation. Hence, any washing step done after exfoliation is likely to affect the thickness measured. It is also unclear if and how different dispersants affect the apparent thickness, by making it impossible to compare works based on different stabilizers. It should be stressed that although many groups have proposed different characterization protocols based on spectroscopic techniques, these methods should be used with awareness of their limitations. We invite the reader to look at other reviews, where the characterization protocols and their limits have been discussed in details.[44,56] Finally, statistical analysis, *i.e.* calculation of the average size and thickness of flakes over a large sample size, should be mandatory as these values provide a valid descriptor of the properties of the dispersion contents. A Raman spectrum or an image taken by AFM may only be representative of the best sample, but not of the whole distribution. It would be ideal to develop a method to measure the thickness of a large number of nanosheets – possibly, to directly detect the number of layers. While AFM can provide quick measurements on a large number of flakes, the uncertainty on the thickness measurement make the method only qualitative. In contrast, electron microscopy is very time consuming and require special sample preparation. The stability of the dispersions should also be reported and evaluated by zeta potential measurements or dynamic light scattering over at least 2 weeks. As discussed, many works do not provide full details on the process (*e.g.* amount of starting bulk material, details on ultrasonication methods, *etc.*) and other works do not report full characterization of the nanosheets, in particular for the less studied 2D materials. It is of crucial importance for the community to provide clear guidelines on which information should be mandatory when reporting results on materials produced by LPE.

Understanding of the exfoliation and stabilization mechanism is of crucial importance to enhance the exfoliation yield, especially in terms of how the dispersant molecules interact with the desired 2D material in the chosen solvent medium. While the general mechanism is clear, *i.e.* the amphiphilic nature of the dispersant shows favourable interaction between its hydrophobic part and the 2D material, whereas the hydrophilic part interacts with the solvent medium, stabilising the dispersant/2D material complex in the solvent medium, the exact interaction of the dispersant with the nanosheets and the solvent is lacking. We must improve our understanding on how the molecular geometry of the dispersant can be used to enhance the adsorption onto the 2D material, on how the chemical composition and structure of 2D materials beyond graphene can affect the interaction with the dispersant and the solvent medium, and on how the kinetics of dispersant adsorption can lead to region-selective adsorption on the 2D material surface or to the discovery of a new dispersant designed specifically for a particular 2D material. In other words, we do not know how molecules are adsorbed on the nanosheets and how they are arranged and which are the factors that play a role in determining their arrangement. The only few experimental studies that have looked at this problem are based on NMR-based techniques. It is hoped that in future advanced techniques, such as NMR and synchrotron-based techniques, will be routinely used for the characterization of the dispersions, possibly *in situ*: this could provide valuable insights on the exfoliation mechanism. Furthermore, certain dispersants may also degrade under prolonged sonication, in particular with tip sonication or due to poor cooling during sonication. As the dispersant amount is minimized with centrifugation, the UV-Vis spectra of the dispersions typically do not show any signal from the dispersant, as well as the Raman spectrum, hence often there is no information on the structure of the dispersant, once adsorbed on the nanosheets. Nanoscale techniques, which are able to identify molecules randomly adsorbed on surfaces, are urgently needed. The knowledge on how many molecules are adsorbed on the nanosheets is also useful for the exploitation of such 2D material dispersions into applications. As the dispersant is an additive, often it is unwanted and needs to be removed by post-processing. Additives, such as pyrene derivatives, typically require temperature above 400 °C to be removed, which is inconvenient in some applications. In such cases, it is crucial to introduce washing steps to minimize free dispersant and to somehow quantify how many molecules are left. The amount of adsorbed stabilizer is also likely to determine the cytotoxicity of the nanosheets. We remark however that in certain applications the dispersant does not need to be removed; in contrast, the dispersant can be used to provide specific properties to the nanosheet. For example, the dispersant can be used to tune surface charge or to introduce specific functional groups to load a drug or to interact with a particular analyte. This review contains many examples of such applications: in the case of BP, the dispersants can improve its stability in air.[190] In another approach, MoS_2 modified with P3TH was used to make hybrid materials with new optical properties due the interaction between MoS_2 and P3HT.[137] BSA was used as dispersant to improve MoS_2 binding capacity to pesticides.[160] With (ss)DNA modification, WSe_2 nanosheets did show excellent antibacterial ability.[161] The drug doxorubicin can be loaded on CS-modified MoS_2.[153]

From our review it is clear that the potential of the dispersant-assisted method has not been fully exploited yet: most of the works refer to TMDs (Table 2), while the family of 2D materials is much larger. There are many questions that remain unanswered, and a wide range of experiments still to perform. For example, based on the recent results reported by our group on highly concentrated graphene dispersions obtained by using insoluble and complex aromatic mole-

cules,[115] it would be interesting to apply this method also to other 2D materials, although the molecule will need to be designed accordingly to the specific 2D material.

Overall, this review has shown that dispersant-assisted LPE is a simple one-pot approach to obtain stable and concentrated dispersions of nanosheets with specific surface charge and chemistry, especially in water. To achieve the full potential of this approach, theoreticians, organic chemists and material scientists need to work together in order to elucidate the fundamentals of the exfoliation process, which in turn will allow to design the best dispersant for a specific class of 2D materials or for a particular application.

Conflicts of interest

There are no conflicts to declare.

Acknowledgements

The authors acknowledge the EPSRC (projects EP/P00119X/1 and EP/N010345/1) and the Lloyd's Register Foundation for financial support.

References

1 A. K. Geim and K. S. Novoselov, *Nat. Mater.*, 2007, **6**, 183–191.
2 A. K. Geim, *Science*, 2009, **324**, 1530–1534.
3 A. H. Castro Neto, F. Guinea, N. M. R. Peres, K. S. Novoselov and A. K. Geim, *Rev. Mod. Phys.*, 2009, **81**, 109–162.
4 K. S. Novoselov, V. I. Fal'ko, L. Colombo, P. R. Gellert, M. G. Schwab and K. Kim, *Nature*, 2012, **490**, 192–200.
5 A. C. Ferrari, F. Bonaccorso, V. Fal'ko, K. S. Novoselov, S. Roche, P. Boggild, S. Borini, F. H. Koppens, V. Palermo, N. Pugno, J. A. Garrido, R. Sordan, A. Bianco, L. Ballerini, M. Prato, E. Lidorikis, J. Kivioja, C. Marinelli, T. Ryhanen, A. Morpurgo, J. N. Coleman, V. Nicolosi and L. Colombo, *Nanoscale*, 2015, **7**, 4598–4810.
6 C. N. R. Rao and A. K. Sood, *Graphene: synthesis, properties, and phenomena*, John Wiley & Sons, 2013.
7 L. E. F. Torres, S. Roche and J.-C. Charlier, *Introduction to graphene-based nanomaterials: from electronic structure to quantum transport*, Cambridge University Press, 2020.
8 H.-S. P. Wong and D. Akinwande, *Carbon nanotube and graphene device physics*, Cambridge University Press, 2011.
9 D. Akinwande, N. Petrone and J. Hone, *Nat. Commun.*, 2014, **5**, 5678.
10 K. S. Novoselov, A. K. Geim, S. V. Morozov, D. Jiang, Y. Zhang, S. V. Dubonos, I. V. Grigorieva and A. A. Firsov, *Science*, 2004, **306**, 666–669.
11 X. Huang, Z. Zeng and H. Zhang, *Chem. Soc. Rev.*, 2013, **42**, 1934–1946.
12 R. Lv, J. A. Robinson, R. E. Schaak, D. Sun, Y. Sun, T. E. Mallouk and M. Terrones, *Acc. Chem. Res.*, 2015, **48**, 56–64.
13 L. H. Li and Y. Chen, *Adv. Funct. Mater.*, 2016, **26**, 2594–2608.
14 H. Liu, Y. Du, Y. Deng and P. D. Ye, *Chem. Soc. Rev.*, 2015, **44**, 2732–2743.
15 V. Eswaraiah, Q. Zeng, Y. Long and Z. Liu, *Small*, 2016, **12**, 3480–3502.
16 S. Das, J. A. Robinson, M. Dubey, H. Terrones and M. Terrones, *Annu. Rev. Mater. Res.*, 2015, **45**, 1–27.
17 S. Z. Butler, S. M. Hollen, L. Cao, Y. Cui, J. A. Gupta, H. R. Gutierrez, T. F. Heinz, S. S. Hong, J. Huang, A. F. Ismach, E. Johnston-Halperin, M. Kuno, V. V. Plashnitsa, R. D. Robinson, R. S. Ruoff, S. Salahuddin, J. Shan, L. Shi, M. G. Spencer, M. Terrones, W. Windl and J. E. Goldberger, *ACS Nano*, 2013, **7**, 2898–2926.
18 Q. Weng, X. Wang, X. Wang, Y. Bando and D. Golberg, *Chem. Soc. Rev.*, 2016, **45**, 3989–4012.
19 N. Mounet, M. Gibertini, P. Schwaller, D. Campi, A. Merkys, A. Marrazzo, T. Sohier, I. E. Castelli, A. Cepellotti, G. Pizzi and N. Marzari, *Nat. Nanotechnol.*, 2018, **13**, 246–252.
20 G. Fiori, F. Bonaccorso, G. Iannaccone, T. Palacios, D. Neumaier, A. Seabaugh, S. K. Banerjee and L. Colombo, *Nat. Nanotechnol.*, 2014, **9**, 768–779.
21 M. Chhowalla, D. Jena and H. Zhang, *Nat. Rev. Mater.*, 2016, **1**, 16052.
22 B. Mendoza-Sánchez and Y. Gogotsi, *Adv. Mater.*, 2016, **28**, 6104–6135.
23 F. Bonaccorso, L. Colombo, G. Yu, M. Stoller, V. Tozzini, A. C. Ferrari, R. S. Ruoff and V. Pellegrini, *Science*, 2015, **347**, 1246501.
24 G. Reina, J. M. Gonzalez-Dominguez, A. Criado, E. Vazquez, A. Bianco and M. Prato, *Chem. Soc. Rev.*, 2017, **46**, 4400–4416.
25 R. Kurapati, K. Kostarelos, M. Prato and A. Bianco, *Adv. Mater.*, 2016, **28**, 6052–6074.
26 Y. Liu, X. Dong and P. Chen, *Chem. Soc. Rev.*, 2012, **41**, 2283–2307.
27 Y. Yang, A. M. Asiri, Z. Tang, D. Du and Y. Lin, *Mater. Today*, 2013, **16**, 365–373.
28 V. Nicolosi, M. Chhowalla, M. G. Kanatzidis, M. S. Strano and J. N. Coleman, *Science*, 2013, **340**, 1226419.
29 J. N. Coleman, M. Lotya, A. O'Neill, S. D. Bergin, P. J. King, U. Khan, K. Young, A. Gaucher, S. De, R. J. Smith, I. V. Shvets, S. K. Arora, G. Stanton, H.-Y. Kim, K. Lee, G. T. Kim, G. S. Duesberg, T. Hallam, J. J. Boland, J. J. Wang, J. F. Donegan, J. C. Grunlan, G. Moriarty, A. Shmeliov, R. J. Nicholls, J. M. Perkins, E. M. Grieveson, K. Theuwissen, D. W. McComb, P. D. Nellist and V. Nicolosi, *Science*, 2011, **331**, 568–571.
30 J. N. Coleman, *Acc. Chem. Res.*, 2013, **46**, 14–22.
31 K. S. Novoselov, D. Jiang, F. Schedin, T. J. Booth, V. V. Khotkevich, S. V. Morozov and A. K. Geim, *Proc. Natl. Acad. Sci. U. S. A.*, 2005, **102**, 10451–10453.

32 J. S. Son, J. H. Yu, S. G. Kwon, J. Lee, J. Joo and T. Hyeon, *Adv. Mater.*, 2011, **23**, 3214–3219.
33 H. Zhang, B. H. Savitzky, J. Yang, J. T. Newman, K. A. Perez, B.-R. Hyun, L. F. Kourkoutis, T. Hanrath and F. W. Wise, *Chem. Mater.*, 2015, **28**, 127–134.
34 Y. Wu, B. Yuan, M. Li, W. H. Zhang, Y. Liu and C. Li, *Chem. Sci.*, 2015, **6**, 1873–1878.
35 C. Tan and H. Zhang, *Nat. Commun.*, 2015, **6**, 7873.
36 M. S. Sokolikova, P. C. Sherrell, P. Palczynski, V. L. Bemmer and C. Mattevi, *Nat. Commun.*, 2019, **10**, 712.
37 T. Kuilla, S. Bhadra, D. Yao, N. H. Kim, S. Bose and J. H. Lee, *Prog. Polym. Sci.*, 2010, **35**, 1350–1375.
38 X. Cao, C. Tan, X. Zhang, W. Zhao and H. Zhang, *Adv. Mater.*, 2016, **28**, 6167–6196.
39 X. Peng, L. Peng, C. Wu and Y. Xie, *Chem. Soc. Rev.*, 2014, **43**, 3303–3323.
40 M. Acerce, D. Voiry and M. Chhowalla, *Nat. Nanotechnol.*, 2015, **10**, 313–318.
41 G. Hu, J. Kang, L. W. T. Ng, X. Zhu, R. C. T. Howe, C. G. Jones, M. C. Hersam and T. Hasan, *Chem. Soc. Rev.*, 2018, **47**, 3265–3300.
42 L. Ng, G. Hu, R. Howe, X. Zhu, Z. Yang, C. G. Jones and T. Hasan, *Printing of Graphene and Related 2D Materials*, Springer, 2018.
43 D. McManus, S. Vranic, F. Withers, V. Sanchez-Romaguera, M. Macucci, H. Yang, R. Sorrentino, K. Parvez, S. K. Son, G. Iannaccone, K. Kostarelos, G. Fiori and C. Casiraghi, *Nat. Nanotechnol.*, 2017, **12**, 343–350.
44 L. Fusco, A. Gazzi, G. Peng, Y. Shin, S. Vranic, D. Bedognetti, F. Vitale, A. Yilmazer, X. Feng, B. Fadeel, C. Casiraghi and L. G. Delogu, *Theranostics*, 2020, **10**, 5435–5488.
45 J. N. Coleman, *Adv. Funct. Mater.*, 2009, **19**, 3680–3695.
46 S. D. Bergin, V. Nicolosi, P. V. Streich, S. Giordani, Z. Sun, A. H. Windle, P. Ryan, N. P. P. Niraj, Z.-T. T. Wang, L. Carpenter, W. J. Blau, J. J. Boland, J. P. Hamilton and J. N. Coleman, *Adv. Mater.*, 2008, **20**, 1876–1881.
47 J. L. Bahr, E. T. Mickelson, M. J. Bronikowski, R. E. Smalley and J. M. Tour, *Chem. Commun.*, 2001, **2**, 193–194.
48 K. D. Ausman, R. Piner, O. Lourie, R. S. Ruoff and M. Korobov, *J. Mater. Chem. B*, 2000, **104**, 8911–8915.
49 C. A. Furtado, U. J. Kim, H. R. Gutierrez, L. Pan, E. C. Dickey and P. C. Eklund, *J. Am. Chem. Soc.*, 2004, **126**, 6095–6105.
50 Y. Maeda, S.-i. Kimura, Y. Hirashima, M. Kanda, Y. Lian, T. Wakahara, T. Akasaka, T. Hasegawa, H. Tokumoto, T. Shimizu, H. Kataura, Y. Miyauchi, S. Maruyama, K. Kobayashi and S. Nagase, *J. Mater. Chem. C*, 2004, **108**, 18395–18397.
51 L. Niu, J. N. Coleman, H. Zhang, H. Shin, M. Chhowalla and Z. Zheng, *Small*, 2016, **12**, 272–293.
52 C. Backes, D. Campi, B. M. Szydlowska, K. Synnatschke, E. Ojala, F. Rashvand, A. Harvey, A. Griffin, Z. Sofer, N. Marzari, J. N. Coleman and D. D. O'Regan, *ACS Nano*, 2019, **13**, 7050–7061.
53 K. Synnatschke, P. A. Cieslik, A. Harvey, A. Castellanos-Gomez, T. Tian, C.-J. Shih, A. Chernikov, E. J. G. Santos, J. N. Coleman and C. Backes, *Chem. Mater.*, 2019, **31**, 10049–10062.
54 U. Khan, A. O'Neill, H. Porwal, P. May, K. Nawaz and J. N. Coleman, *Carbon*, 2012, **50**, 470–475.
55 A. Griffin, A. Harvey, B. Cunningham, D. Scullion, T. Tian, C.-J. Shih, M. Gruening, J. F. Donegan, E. J. G. Santos, C. Backes and J. N. Coleman, *Chem. Mater.*, 2018, **30**, 1998–2005.
56 C. Backes, T. M. Higgins, A. Kelly, C. Boland, A. Harvey, D. Hanlon and J. N. Coleman, *Chem. Mater.*, 2017, **29**, 243–255.
57 C. Backes, A. M. Abdelkader, C. Alonso, A. Andrieux-Ledier, R. Arenal, J. Azpeitia, N. Balakrishnan, L. Banszerus, J. Barjon and R. Bartali, *2D Mater.*, 2020, **7**, 022001.
58 Y. Hernandez, V. Nicolosi, M. Lotya, F. M. Blighe, Z. Sun, S. De, I. T. McGovern, B. Holland, M. Byrne, Y. K. Gun'Ko, J. J. Boland, P. Niraj, G. Duesberg, S. Krishnamurthy, R. Goodhue, J. Hutchison, V. Scardaci, A. C. Ferrari and J. N. Coleman, *Nat. Nanotechnol.*, 2008, **3**, 563–568.
59 J. Kim, S. Kwon, D.-H. Cho, B. Kang, H. Kwon, Y. Kim, S. O. Park, G. Y. Jung, E. Shin, W.-G. Kim, H. Lee, G. H. Ryu, M. Choi, T. H. Kim, J. Oh, S. Park, S. K. Kwak, S. W. Yoon, D. Byun, Z. Lee and C. Lee, *Nat. Commun.*, 2015, **6**, 8294.
60 A. Ciesielski and P. Samori, *Chem. Soc. Rev.*, 2014, **43**, 381–398.
61 S. Wang, M. Yi and Z. Shen, *RSC Adv.*, 2016, **6**, 56705–56710.
62 M. Yi and Z. Shen, *J. Mater. Chem. A*, 2015, **3**, 11700–11715.
63 L. Liu, Z. Shen, M. Yi, X. Zhang and S. Ma, *RSC Adv.*, 2014, **4**, 36464–36470.
64 V. Leon, M. Quintana, M. A. Herrero, J. L. Fierro, A. de la Hoz, M. Prato and E. Vazquez, *Chem. Commun.*, 2011, **47**, 10936–10938.
65 V. Leon, A. M. Rodriguez, P. Prieto, M. Prato and E. Vazquez, *ACS Nano*, 2014, **8**, 563–571.
66 P. G. Karagiannidis, S. A. Hodge, L. Lombardi, F. Tomarchio, N. Decorde, S. Milana, I. Goykhman, Y. Su, S. V. Mesite and D. N. Johnstone, *ACS Nano*, 2017, **11**, 2742–2755.
67 H. Tao, Y. Zhang, Y. Gao, Z. Sun, C. Yan and J. Texter, *Phys. Chem. Chem. Phys.*, 2017, **19**, 921–960.
68 Y. Hernandez, M. Lotya, D. Rickard, S. D. Bergin and J. N. Coleman, *Langmuir*, 2010, **26**, 3208–3213.
69 U. Khan, A. O'Neill, M. Lotya, S. De and J. N. Coleman, *Small*, 2010, **6**, 864–871.
70 J. N. Spencer, G. M. Bodner and L. H. Rickard, *Chemistry: structure and dynamics*, John Wiley & Sons, 2010.
71 J. Lyklema, *Colloids Surf., A*, 1999, **156**, 413–421.
72 C. M. Hansen, *Hansen solubility parameters: a user's handbook*, CRC press, 2007.
73 K. G. Zhou, N. N. Mao, H. X. Wang, Y. Peng and H. L. Zhang, *Angew. Chem., Int. Ed.*, 2011, **50**, 10839–10842.

74 Y. Lin, T. V. Williams, T.-B. Xu, W. Cao, H. E. Elsayed-Ali and J. W. Connell, *J. Phys. Chem. C*, 2011, **115**, 2679–2685.
75 B. Derjaguin and L. Landau, *Prog. Surf. Sci.*, 1993, **43**, 30–59.
76 S. Haar, A. Ciesielski, J. Clough, H. Yang, R. Mazzaro, F. Richard, S. Conti, N. Merstorf, M. Cecchini and V. J. S. Morandi, *Small*, 2015, **11**, 1691–1702.
77 J. Geng, B.-S. Kong, S. B. Yang and H.-T. Jung, *Chem. Commun.*, 2010, **46**, 5091–5093.
78 Y. T. Liang and M. C. Hersam, *J. Am. Chem. Soc.*, 2010, **132**, 17661–17663.
79 L. Xu, J.-W. McGraw, F. Gao, M. Grundy, Z. Ye, Z. Gu and J. L. Shepherd, *J. Phys. Chem. C*, 2013, **117**, 10730–10742.
80 S. Haar, M. El Gemayel, Y. Shin, G. Melinte, M. A. Squillaci, O. Ersen, C. Casiraghi, A. Ciesielski and P. Samorì, *Sci. Rep.*, 2015, **5**, 16684.
81 S. Haar, M. Bruna, J. X. Lian, F. Tomarchio, Y. Olivier, R. Mazzaro, V. Morandi, J. Moran, A. C. Ferrari and D. Beljonne, *J. Phys. Chem. Lett.*, 2016, **7**, 2714–2721.
82 A. Liscio, K. Kouroupis-Agalou, A. Kovtun, E. Gebremedhn, M. El Garah, W. Rekab, E. Orgiu, L. Giorgini, P. Samorì and D. Beljonne, *ChemPlusChem*, 2017, **82**, 358–367.
83 D. J. Shaw, *Introduction to Colloid and Surface Chemistry*, Butterworths, 1980.
84 M. J. O'Connell, S. M. Bachilo, C. B. Huffman, V. C. Moore, M. S. Strano, E. H. Haroz, K. L. Rialon, P. J. Boul, W. H. Noon, C. Kittrell, J. Ma, R. H. Hauge, R. B. Weisman and R. E. Smalley, *Science*, 2002, **297**, 593–596.
85 M. Lotya, Y. Hernandez, P. J. King, R. J. Smith, V. Nicolosi, L. S. Karlsson, F. M. Blighe, S. De, Z. Wang, I. T. McGovern, G. S. Duesberg and J. N. Coleman, *J. Am. Chem. Soc.*, 2009, **131**, 3611–3620.
86 S. De, P. J. King, M. Lotya, A. O'Neill, E. M. Doherty, Y. Hernandez, G. S. Duesberg and J. N. Coleman, *Small*, 2010, **6**, 458–464.
87 M. Lotya, P. J. King, U. Khan, S. De and J. N. Coleman, *ACS Nano*, 2010, **4**, 3155–3162.
88 A. G. Hsieh, S. Korkut, C. Punckt and I. A. Aksay, *Langmuir*, 2013, **29**, 14831–14838.
89 A. Griffin, K. Nisi, J. Pepper, A. Harvey, B. M. Szydłowska, J. N. Coleman and C. Backes, *Chem. Mater.*, 2020, **32**, 2852–2862.
90 P. May, U. Khan, J. M. Hughes and J. N. Coleman, *J. Phys. Chem. C*, 2012, **116**, 11393–11400.
91 L. Guardia, M. J. Fernández-Merino, J. I. Paredes, P. Solís-Fernández, S. Villar-Rodil, A. Martínez-Alonso and J. M. D. Tascón, *Carbon*, 2011, **49**, 1653–1662.
92 A. B. Bourlinos, V. Georgakilas, R. Zboril, T. A. Steriotis, A. K. Stubos and C. Trapalis, *Solid State Commun.*, 2009, **149**, 2172–2176.
93 S. Perumal, K. T. Park, H. M. Lee and I. W. Cheong, *J. Colloid Interface Sci.*, 2016, **464**, 25–35.
94 I. U. Unalan, C. Wan, S. Trabattoni, L. Piergiovanni and S. Farris, *RSC Adv.*, 2015, **5**, 26482–26490.
95 J. Jagiello, J. Judek, M. Zdrojek, M. Aksienionek and L. Lipinska, *Mater. Chem. Phys.*, 2014, **148**, 507–511.
96 S. Zhao, S. Xie, Z. Zhao, J. Zhang, L. Li and Z. Xin, *ACS Sustainable Chem. Eng.*, 2018, **6**, 7652–7661.
97 W. Liu, R. Zhou, D. Zhou, G. Ding, J. M. Soah, C. Y. Yue and X. Lu, *Carbon*, 2015, **83**, 188–197.
98 J. I. Paredes and S. Villar-Rodil, *Nanoscale*, 2016, **8**, 15389–15413.
99 D. Parviz, S. Das, H. S. Ahmed, F. Irin, S. Bhattacharia and M. J. Green, *ACS Nano*, 2012, **6**, 8857–8867.
100 H. Yang, Y. Hernandez, A. Schlierf, A. Felten, A. Eckmann, S. Johal, P. Louette, J. J. Pireaux, X. Feng, K. Mullen, V. Palermo and C. Casiraghi, *Carbon*, 2013, **53**, 357–365.
101 H. Yang, F. Withers, E. Gebremedhn, E. Lewis, L. Britnell, A. Felten, V. Palermo, S. Haigh, D. Beljonne and C. Casiraghi, *2D Mater.*, 2014, **1**, 011012.
102 X. An, T. Simmons, R. Shah, C. Wolfe, K. M. Lewis, M. Washington, S. K. Nayak, S. Talapatra and S. Kar, *Nano Lett.*, 2010, **10**, 4295–4301.
103 S. Bose, T. Kuila, A. K. Mishra, N. H. Kim and J. H. Lee, *Nanotechnology*, 2011, **22**, 405603.
104 A. Ghosh, K. V. Rao, S. J. George and C. N. Rao, *Chemistry*, 2010, **16**, 2700–2704.
105 S. Conti, M. G. del Rosso, A. Ciesielski, J. Weippert, A. Bottcher, Y. Shin, G. Melinte, O. Ersen, C. Casiraghi, X. Feng, K. Mullen, M. M. Kappes, P. Samori and M. Cecchini, *ChemPhysChem*, 2016, **17**, 352–357.
106 A. Hirsch, J. M. Englert and F. Hauke, *Acc. Chem. Res.*, 2013, **46**, 87–96.
107 S. Sampath, A. N. Basuray, K. J. Hartlieb, T. Aytun, S. I. Stupp and J. F. Stoddart, *Adv. Mater.*, 2013, **25**, 2740–2745.
108 A. Schlierf, H. Yang, E. Gebremedhn, E. Treossi, L. Ortolani, L. Chen, A. Minoia, V. Morandi, P. Samori, C. Casiraghi, D. Beljonne and V. Palermo, *Nanoscale*, 2013, **5**, 4205–4216.
109 Y. Shin, X. Just-Baringo, M. Zarattini, L. H. Isherwood, A. Baidak, K. Kostarelos, I. Larrosa and C. Casiraghi, *Mol. Syst. Des. Eng.*, 2019, **4**, 503–510.
110 Y. Shin, S. Vranic, X. Just-Baringo, S. M. Gali, T. Kisby, Y. Chen, A. Gkoutzidou, E. Prestat, D. Beljonne, I. Larrosa, K. Kostarelos and C. Casiraghi, *Nanoscale*, 2020, **12**, 12383–12394.
111 K. W. J. Heard, C. Bartlam, C. D. Williams, J. Zhang, A. A. Alwattar, M. S. Little, A. V. S. Parry, F. M. Porter, M. A. Vincent, I. H. Hillier, F. R. Siperstein, A. Vijayaraghavan, S. G. Yeates and P. Quayle, *ACS Omega*, 2019, **4**, 1969–1981.
112 D. W. Lee, T. Kim and M. Lee, *Chem. Commun.*, 2011, **47**, 8259–8261.
113 W. Li, D. McManus, H. Liu, C. Casiraghi and S. J. Webb, *Phys. Chem. Chem. Phys.*, 2017, **19**, 17036–17043.
114 M. Zhang, R. R. Parajuli, D. Mastrogiovanni, B. Dai, P. Lo, W. Cheung, R. Brukh, P. L. Chiu, T. Zhou, Z. Liu, E. Garfunkel and H. He, *Small*, 2010, **6**, 1100–1107.
115 Y. Shin, X. Just-Baringo, M. Boyes, A. Panigrahi, M. Zarattini, Y. Chen, X. Liu, G. Morris, E. Prestat,

K. Kostarelos, S. Vranic, I. Larrosa and C. Casiraghi, *Faraday Discuss.*, DOI: 10.1039/C9FD00114J.
116 M. Chhowalla, H. S. Shin, G. Eda, L. J. Li, K. P. Loh and H. Zhang, *Nat. Chem.*, 2013, **5**, 263–275.
117 R. J. Smith, P. J. King, M. Lotya, C. Wirtz, U. Khan, S. De, A. O'Neill, G. S. Duesberg, J. C. Grunlan, G. Moriarty, J. Chen, J. Wang, A. I. Minett, V. Nicolosi and J. N. Coleman, *Adv. Mater.*, 2011, **23**, 3944–3948.
118 E. Varrla, C. Backes, K. R. Paton, A. Harvey, Z. Gholamvand, J. McCauley and J. N. Coleman, *Chem. Mater.*, 2015, **27**, 1129–1139.
119 C. Backes, R. J. Smith, N. McEvoy, N. C. Berner, D. McCloskey, H. C. Nerl, A. O'Neill, P. J. King, T. Higgins, D. Hanlon, N. Scheuschner, J. Maultzsch, L. Houben, G. S. Duesberg, J. F. Donegan, V. Nicolosi and J. N. Coleman, *Nat. Commun.*, 2014, **5**, 4576.
120 Y. J. Lee, L. Huang, H. Wang, M. L. Sushko, B. Schwenzer, I. A. Aksay and J. Liu, *Colloids Interface Sci. Commun.*, 2015, **8**, 1–5.
121 P. Ramalingam, S. T. Pusuluri, S. Periasamy, R. Veerabahu and J. Kulandaivel, *RSC Adv.*, 2013, **3**, 2369–2378.
122 Z. Gholamvand, D. McAteer, C. Backes, N. McEvoy, A. Harvey, N. C. Berner, D. Hanlon, C. Bradley, I. Godwin, A. Rovetta, M. E. Lyons, G. S. Duesberg and J. N. Coleman, *Nanoscale*, 2016, **8**, 5737–5749.
123 S. Ott, N. Wolff, F. Rashvand, V. J. Rao, J. Zaumseil and C. Backes, *Chem. Mater.*, 2019, **31**, 8424–8431.
124 D. Mao, B. Du, D. Yang, S. Zhang, Y. Wang, W. Zhang, X. She, H. Cheng, H. Zeng and J. Zhao, *Small*, 2016, **12**, 1489–1497.
125 R. C. T. Howe, R. I. Woodward, G. Hu, Z. Yang, E. J. R. Kelleher and T. Hasan, *Phys. Status Solidi B*, 2016, **253**, 911–917.
126 A. Gupta, V. Arunachalam and S. Vasudevan, *J. Phys. Chem. Lett.*, 2015, **6**, 739–744.
127 A. Gupta and S. Vasudevan, *J. Phys. Chem. C*, 2018, **122**, 19243–19250.
128 S. Grieger, B. M. Szydłowska, V. Rao, E. Steinmann, M. Dodds, Z. Gholamvand, G. S. Duesberg, J. Zaumseil and C. Backes, *Angew. Chem.*, 2020, **59**, 13785–13792.
129 S. Lin, C.-J. Shih, M. S. Strano and D. Blankschtein, *J. Am. Chem. Soc.*, 2011, **133**, 12810–12823.
130 S. Vera-López, P. Martínez, M. San Andrés, A. Díez-Pascual and M. Valiente, *J. Colloid Interface Sci.*, 2018, **514**, 415–424.
131 C. Backes, B. M. Szydlowska, A. Harvey, S. Yuan, V. Vega-Mayoral, B. R. Davies, P. L. Zhao, D. Hanlon, E. J. Santos, M. I. Katsnelson, W. J. Blau, C. Gadermaier and J. N. Coleman, *ACS Nano*, 2016, **10**, 1589–1601.
132 L.-J. Ji, Y. Qin, D. Gui, W. Li, Y. Li, X. Li and P. Lu, *Chem. Mater.*, 2018, **30**, 8732–8738.
133 R. J. Smith, M. Lotya and J. N. Coleman, *New J. Phys.*, 2010, **12**, 125008.
134 J. Liu, Z. Zeng, X. Cao, G. Lu, L. H. Wang, Q. L. Fan, W. Huang and H. Zhang, *Small*, 2012, **8**, 3517–3522.
135 R. Bari, D. Parviz, F. Khabaz, C. D. Klaassen, S. D. Metzler, M. J. Hansen, R. Khare and M. J. Green, *Phys. Chem. Chem. Phys.*, 2015, **17**, 9383–9393.
136 V. Vega-Mayoral, C. Backes, D. Hanlon, U. Khan, Z. Gholamvand, M. O'Brien, G. S. Duesberg, C. Gadermaier and J. N. Coleman, *Adv. Funct. Mater.*, 2016, **26**, 1028–1039.
137 M. Zhao, M. J. Chang, Q. Wang, Z. T. Zhu, X. P. Zhai, M. Zirak, A. Z. Moshfegh, Y. L. Song and H. L. Zhang, *Chem. Commun.*, 2015, **51**, 12262–12265.
138 L. Guardia, J. I. Paredes, R. Rozada, S. Villar-Rodil, A. Martínez-Alonso and J. M. D. Tascón, *RSC Adv.*, 2014, **4**, 14115–14127.
139 N. D. Mansukhani, L. M. Guiney, P. J. Kim, Y. Zhao, D. Alducin, A. Ponce, E. Larios, M. J. Yacaman and M. C. Hersam, *Small*, 2016, **12**, 294–300.
140 S. Xu, H. Zheng, R. Ma, D. Wu, Y. Pan, C. Yin, M. Gao, W. Wang, W. Li, S. Liu, Z. Chai and R. Li, *Nat. Commun.*, 2020, **11**, 3484.
141 M. D. Quinn, N. H. Ho and S. M. Notley, *ACS Appl. Mater. Interfaces*, 2013, **5**, 12751–12756.
142 S. M. Notley, *Langmuir*, 2012, **28**, 14110–14113.
143 J. Kang, J. W. Seo, D. Alducin, A. Ponce, M. J. Yacaman and M. C. Hersam, *Nat. Commun.*, 2014, **5**, 5478.
144 F. Bonaccorso, T. Hasan, P. H. Tan, C. Sciascia, G. Privitera, G. Di Marco, P. G. Gucciardi and A. C. Ferrari, *J. Phys. Chem. C*, 2010, **114**, 17267–17285.
145 P. Zhao, E. Einarsson, G. Lagoudas, J. Shiomi, S. Chiashi and S. Maruyama, *Nano Res.*, 2011, **4**, 623–634.
146 M. S. Arnold, S. I. Stupp and M. C. Hersam, *Nano Lett.*, 2005, **5**, 713–718.
147 A. A. Green and M. C. Hersam, *Adv. Mater.*, 2011, **23**, 2185–2190.
148 X. Sun, D. Luo, J. Liu and D. G. Evans, *ACS Nano*, 2010, **4**, 3381–3389.
149 A. A. Green and M. C. Hersam, *J. Phys. Chem. Lett.*, 2010, **1**, 544–549.
150 D. Wang, L. Song, K. Zhou, X. Yu, Y. Hu and J. Wang, *J. Mater. Chem. A*, 2015, **3**, 14307–14317.
151 X. Feng, X. Wang, W. Xing, K. Zhou, L. Song and Y. Hu, *Compos. Sci. Technol.*, 2014, **93**, 76–82.
152 M. Fang, J. Long, W. Zhao, L. Wang and G. Chen, *Langmuir*, 2010, **26**, 16771–16774.
153 W. Yin, L. Yan, J. Yu, G. Tian, L. Zhou, X. Zheng, X. Zhang, Y. Yong, J. Li, Z. Gu and Y. Zhao, *ACS Nano*, 2014, **8**, 6922–6933.
154 S. S. Chou, B. Kaehr, J. Kim, B. M. Foley, M. De, P. E. Hopkins, J. Huang, C. J. Brinker and V. P. Dravid, *Angew. Chem., Int. Ed.*, 2013, **52**, 4160–4164.
155 X. Y. Wong, A. Sena-Torralba, R. Álvarez-Diduk, K. Muthoosamy and A. Merkoçi, *ACS Nano*, 2020, **14**, 2585–2627.
156 Y. Li, H. Zhu, F. Shen, J. Wan, S. Lacey, Z. Fang, H. Dai and L. Hu, *Nano Energy*, 2015, **13**, 346–354.
157 W. Liu, C. Zhao, R. Zhou, D. Zhou, Z. Liu and X. Lu, *Nanoscale*, 2015, **7**, 9919–9926.

158 Y. Ge, J. Wang, Z. Shi and J. Yin, *J. Mater. Chem.*, 2012, **22**, 17619–17624.
159 S. Ravula, J. B. Essner and G. A. Baker, *ChemNanoMat*, 2015, **1**, 167–177.
160 G. Guan, S. Zhang, S. Liu, Y. Cai, M. Low, C. P. Teng, I. Y. Phang, Y. Cheng, K. L. Duei, B. M. Srinivasan, Y. Zheng, Y. W. Zhang and M. Y. Han, *J. Am. Chem. Soc.*, 2015, **137**, 6152–6155.
161 G. S. Bang, S. Cho, N. Son, G. W. Shim, B. K. Cho and S. Y. Choi, *ACS Appl. Mater. Interfaces*, 2016, **8**, 1943–1950.
162 D. McManus, A. Dal Santo, P. B. Selvasundaram, R. Krupke, A. LiBassi and C. Casiraghi, *Flexible Printed Electron.*, 2018, **3**, 034005.
163 T. Leng, K. Parvez, K. Pan, J. Ali, D. McManus, K. S. Novoselov, C. Casiraghi and Z. Hu, *2D Mater.*, 2020, **7**, 024004.
164 X. Wu, Y. Li, L. Chen, J. Zhao, B. Wu and Z. B. Zhang, *Chem. Commun.*, 2020, **56**, 2035–2038.
165 Y. X. Chen, C. W. Wu, T. Y. Kuo, Y. L. Chang, M. H. Jen and I. W. Chen, *Sci. Rep.*, 2016, **6**, 26660.
166 X. Chen, R. A. Boulos, P. K. Eggers and C. L. Raston, *Chem. Commun.*, 2012, **48**, 11407–11409.
167 F. Zhang, X. Chen, R. A. Boulos, F. M. Yasin, H. Lu, C. Raston and H. Zhang, *Chem. Commun.*, 2013, **49**, 4845–4847.
168 B. Mao, Y. Yuan, Y. Shao, B. Yang, Z. Xiao and J. Huang, *Nanosci. Nanotechnol. Lett.*, 2014, **6**, 685–691.
169 R. Anbazhagan, H.-J. Wang, H.-C. Tsai and R.-J. Jeng, *RSC Adv.*, 2014, **4**, 42936–42941.
170 M. Ayan-Varela, O. Perez-Vidal, J. I. Paredes, J. M. Munuera, S. Villar-Rodil, M. Diaz-Gonzalez, C. Fernandez-Sanchez, V. S. Silva, M. Cicuendez, M. Vila, A. Martinez-Alonso and J. M. Tascon, *ACS Appl. Mater. Interfaces*, 2017, **9**, 2835–2845.
171 E. Long, S. O'Brien, E. A. Lewis, E. Prestat, C. Downing, C. S. Cucinotta, S. Sanvito, S. J. Haigh and V. Nicolosi, *2D Mater. Appl.*, 2017, **1**, 22.
172 V. Vega-Mayoral, R. Tian, A. G. Kelly, A. Griffin, A. Harvey, M. Borrelli, K. Nisi, C. Backes and J. N. Coleman, *Nanoscale*, 2019, **11**, 6206–6216.
173 J. Kang, V. K. Sangwan, J. D. Wood, X. Liu, I. Balla, D. Lam and M. C. Hersam, *Nano Lett.*, 2016, **16**, 7216–7223.
174 W.-Q. Han, L. Wu, Y. Zhu, K. Watanabe and T. Taniguchi, *Appl. Phys. Lett.*, 2008, **93**, 223103.
175 C. Zhi, Y. Bando, C. Tang, H. Kuwahara and D. Golberg, *Adv. Mater.*, 2009, **21**, 2889–2893.
176 A. Chae, S.-J. Park, B. Min and I. In, *Mater. Res. Express*, 2018, **5**, 015036.
177 J. Zhu, J. Kang, J. Kang, D. Jariwala, J. D. Wood, J. W. Seo, K. S. Chen, T. J. Marks and M. C. Hersam, *Nano Lett.*, 2015, **15**, 7029–7036.
178 J. Biscarat, M. Bechelany, C. Pochat-Bohatier and P. Miele, *Nanoscale*, 2015, **7**, 613–618.
179 R. Worsley, L. Pimpolari, D. McManus, N. Ge, R. Ionescu, J. A. Wittkopf, A. Alieva, G. Basso, M. Macucci, G. Iannaccone, K. S. Novoselov, H. Holder, G. Fiori and C. Casiraghi, *ACS Nano*, 2019, **13**, 54–60.
180 A. Brown and S. Rundqvist, *Acta Crystallogr.*, 1965, **19**, 684–685.
181 L. Li, Y. Yu, G. J. Ye, Q. Ge, X. Ou, H. Wu, D. Feng, X. H. Chen and Y. Zhang, *Nat. Nanotechnol.*, 2014, **9**, 372–377.
182 G. Abellan, S. Wild, V. Lloret, N. Scheuschner, R. Gillen, U. Mundloch, J. Maultzsch, M. Varela, F. Hauke and A. Hirsch, *J. Am. Chem. Soc.*, 2017, **139**, 10432–10440.
183 A. Favron, E. Gaufres, F. Fossard, A. L. Phaneuf-L'Heureux, N. Y. Tang, P. L. Levesque, A. Loiseau, R. Leonelli, S. Francoeur and R. Martel, *Nat. Mater.*, 2015, **14**, 826–832.
184 D. Hanlon, C. Backes, E. Doherty, C. S. Cucinotta, N. C. Berner, C. Boland, K. Lee, A. Harvey, P. Lynch, Z. Gholamvand, S. Zhang, K. Wang, G. Moynihan, A. Pokle, Q. M. Ramasse, N. McEvoy, W. J. Blau, J. Wang, G. Abellan, F. Hauke, A. Hirsch, S. Sanvito, D. D. O'Regan, G. S. Duesberg, V. Nicolosi and J. N. Coleman, *Nat. Commun.*, 2015, **6**, 8563.
185 J. Kang, J. D. Wood, S. A. Wells, J.-H. Lee, X. Liu, K.-S. Chen and M. C. Hersam, *ACS Nano*, 2015, **9**, 3596–3604.
186 P. Yasaei, B. Kumar, T. Foroozan, C. Wang, M. Asadi, D. Tuschel, J. E. Indacochea, R. F. Klie and A. Salehi-Khojin, *Adv. Mater.*, 2015, **27**, 1887–1892.
187 A. H. Woomer, T. W. Farnsworth, J. Hu, R. A. Wells, C. L. Donley and S. C. Warren, *ACS Nano*, 2015, **9**, 8869–8884.
188 J. Kang, S. A. Wells, J. D. Wood, J.-H. Lee, X. Liu, C. R. Ryder, J. Zhu, J. R. Guest, C. A. Husko and M. C. Hersam, *Proc. Natl. Acad. Sci. U. S. A.*, 2016, **113**, 11688–11693.
189 R. Gusmao, Z. Sofer and M. Pumera, *ACS Nano*, 2018, **12**, 5666–5673.
190 R. Jain, Y. Singh, S.-Y. Cho, S. P. Sasikala, S. H. Koo, R. Narayan, H.-T. Jung, Y. Jung and S. O. Kim, *Chem. Mater.*, 2019, **31**, 2786–2794.
191 Y. Zhang, N. Dong, H. Tao, C. Yan, J. Huang, T. Liu, A. W. Robertson, J. Texter, J. Wang and Z. Sun, *Chem. Mater.*, 2017, **29**, 6445–6456.
192 J. Peng, Y. Lai, Y. Chen, J. Xu, L. Sun and J. Weng, *Small*, 2017, **13**, 1603589.
193 W. Zhao, Z. Xue, J. Wang, J. Jiang, X. Zhao and T. Mu, *ACS Appl. Mater. Interfaces*, 2015, **7**, 27608–27612.
194 M. Lee, A. K. Roy, S. Jo, Y. Choi, A. Chae, B. Kim, S. Y. Park and I. In, *Nanotechnology*, 2017, **28**, 125603.
195 V. V. Chaban, E. E. Fileti and O. V. Prezhdo, *ACS Nano*, 2017, **11**, 6459–6466.
196 C.-X. Hu, Q. Xiao, Y.-Y. Ren, M. Zhao, G.-H. Dun, H.-R. Wu, X.-Y. Li, Q.-Q. Yang, B. Sun, Y. Peng, F. Yan, Q. Wang and H.-L. Zhang, *Adv. Funct. Mater.*, 2018, **28**, 1805311.
197 J. Y. Xu, L. F. Gao, C. X. Hu, Z. Y. Zhu, M. Zhao, Q. Wang and H. L. Zhang, *Chem. Commun.*, 2016, **52**, 8107–8110.

198 W. Cai, T. Cai, L. He, F. Chu, X. Mu, L. Han, Y. Hu, B. Wang and W. Hu, *J. Hazard. Mater.*, 2020, **387**, 121971.
199 G. Pizzi, M. Gibertini, E. Dib, N. Marzari, G. Iannaccone and G. Fiori, *Nat. Commun.*, 2016, **7**, 12585.
200 M. Pumera and Z. Sofer, *Adv. Mater.*, 2017, **29**, 1605299.
201 S. Zhang, W. Zhou, Y. Ma, J. Ji, B. Cai, S. A. Yang, Z. Zhu, Z. Chen and H. Zeng, *Nano Lett.*, 2017, **17**, 3434–3440.
202 Q. Xiao, C.-X. Hu, H.-R. Wu, Y.-Y. Ren, X.-Y. Li, Q.-Q. Yang, G.-H. Dun, Z.-P. Huang, Y. Peng, F. Yan, Q. Wang and H.-L. Zhang, *Nanoscale Horiz.*, 2020, **5**, 124–130.
203 Q. Wang and D. O'Hare, *Chem. Rev.*, 2012, **112**, 4124–4155.
204 D. McAteer, I. J. Godwin, Z. Ling, A. Harvey, L. He, C. S. Boland, V. Vega-Mayoral, B. Szydłowska, A. A. Rovetta and C. Backes, *Adv. Energy Mater.*, 2018, **8**, 1702965.
205 A. Harvey, X. He, I. J. Godwin, C. Backes, D. McAteer, N. C. Berner, N. McEvoy, A. Ferguson, A. Shmeliov, M. E. G. Lyons, V. Nicolosi, G. S. Duesberg, J. F. Donegan and J. N. Coleman, *J. Mater. Chem. A*, 2016, **4**, 11046–11059.
206 A. Harvey, C. Backes, J. B. Boland, X. He, A. Griffin, B. Szydlowska, C. Gabbett, J. F. Donegan and J. N. Coleman, *Nat. Commun.*, 2018, **9**, 4553.
207 A. Harvey, J. B. Boland, I. Godwin, A. G. Kelly, B. M. Szydłowska, G. Murtaza, A. Thomas, D. J. Lewis, P. O'Brien and J. N. Coleman, *2D Mater.*, 2017, **4**, 025054.